DEPARTMENT OF THE AIR FORCE
HEADQUARTERS AIR FORCE DEVELOPMENT TEST CENTER (AFMC)
EGLIN AIR FORCE BASE, FLORIDA

SSN 396

27 March 1996

MEMORANDUM FOR WL/CA-N
ATTN: DR. MIN

FROM: AFDTC/PA

SUBJECT: Clearance for Public Release

The technical note "Development of a Reflector IRA and a Solid Dielectric IRA, Part I: Design, Prediction, and Construction" has been reviewed. Public release is approved.

Jim I Swinson Jr

JIM I. SWINSON JR
Security & Policy Review
Office of Public Affairs

Atch:
Tech Note

AFDTC/PA 96-123

Sensor and Simulation Notes

Note 396

Development of a Reflector IRA and a Solid Dielectric Lens IRA, Part I: Design, Predictions, and Construction

April 1996

Everett G. Farr
Farr Research

Charles A. Frost
Pulse Power Physics

Abstract

In this note we begin the development of two types of Impulse Radiating Antenna (IRA). These two designs include a 23 cm diameter reflector IRA, with an *F/D* of 0.38, and a solid dielectric-lens IRA, or dielectric-immersed lens IRA. This latter design is a Transverse Electromagnetic (TEM) horn immersed in a dielectric, with a prolate spheroidal lens interface to air. The reflector IRA consists of a paraboloidal reflector, fed by a conical 4-arm feed, whose combined input impedance is 200 Ω. The lens IRA was constructed from a solid block of polyethylene, conical in shape, and capped by a prolate spheroid. It can be short, because of the prolate spheroidal lens. In addition, since the TEM feed is filled with dielectric, it will provide a better match to 50 Ω, when compared to an air-filled TEM horn with a lens. Since there are fewer dielectric interfaces with this design, there will also be fewer reflections, which reduces Fresnel loss.

The technique for calculating the step response antenna pattern involves calculation of the line integrals of the quasistatic potential over the aperture. The resulting step responses are then convolved with the derivative of the driving voltage to obtain the overall waveshape. The reflector configuration was calculated using a 4-wire approximation to the aperture. The lens IRA was calculated under the assumption that the aperture was that of a TEM horn built with circular plates.

The antenna pattern measurement technique involves using two identical antennas, and we present here the relevant equations for the signal processing. In particular, signal processing techniques are described for extracting the single-antenna response from the 2-antenna measurement. The actual measurements will be presented in a later paper, which will be Part II of this note.

I. Introduction

This report summarizes the design and analysis phase of the development of a Reflector IRA and a Solid Dielectric Lens IRA. We consider first the Reflector IRA, including design equations, the specific design chosen, boresight and off-boresight radiated field, and received voltage for two identical antennas. Next, we consider the same set of issues concerning the lens IRA, and we also consider the possibility of approximating the elliptical surface with a spherical surface. In addition, we consider adaptive noise filters as a technique to enhance our calculation of the antenna step response. Finally, we consider signal propagation through cables, including a simple model of skin effect losses.

We begin with the Reflector IRA.

II. Reflector IRA

We will be building a reflector IRA with a diameter of 23 cm and an F/D ratio of $f_d = 0.3778$. Below we describe the design equations required.

A. Design Equations

The most interesting portion of the design of the reflector IRA deals with the feed arm angles, as shown in Figure 1.A.1. The center angle is specified as

$$\beta = \arctan\left(\frac{1}{2f_d - 1/(8f_d)}\right) \tag{2.A.1}$$

Furthermore, the feed impedance of TEM feed is [1]

$$f_g = \frac{K(m)}{K(1-m)} \tag{2.A.2}$$

where $K(m)$ is the complete elliptic integral of the first kind. For the usual case of the feed impedance being 400 Ω, we have m=0.565291. Having solved for m and β, one then finds the remaining angles as [1]

$$\begin{aligned} \beta_1 &= 2\arctan\left[\, m^{1/4}\tan(\beta/2)\right] \\ \beta_2 &= 2\arctan\left[m^{-1/4}\tan(\beta/2)\right] \end{aligned} \tag{2.A.3}$$

The angles for $f_d = 0.3778$ are now simple to determine. We find β_1, β and β_2 are 59.69, 66.99, 74.70 degrees, respectively.

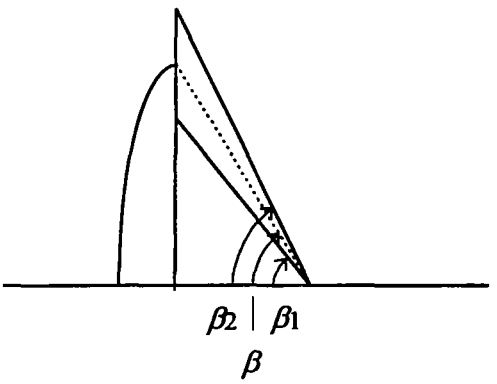

Figure 1.A.1. Angles for specifying the feed arm configuration.

B. Construction Details for the Reflector IRA

Having specified the feed arm angles in the previous section, all that is left is to specify the antenna's *F/D* ratio and its diameter. For this antenna we used $f_d = 0.3778$, with a diameter of 23 cm. A four-arm design was chosen, so the input impedance of the antenna is 200 Ω. The paraboloidal reflector is made of a honeycomb form of a material called Nomex, which is both lightweight and very sturdy. The Nomex honeycomb is covered by a fine copper screen.

The design drawings for the antenna are shown in Figures 2.B.1 - 2.B.2. Pictures of the resulting antennas are in Figure 2.B.3. Initial Time Domain Reflectometry (TDR) measurements indicate a much smoother match to the input line than what was achieved previously in [2].

We have built two impedance matching networks to match the antennas, which have a 200 Ω input impedance, to a 50 Ω cable. First, we used the standard balun, which uses two 100 Ω cables connected in parallel at the input and in series at the output [2,13]. This balun, shown on the left in Figure 2.B.3, requires a fairly large geometry at the apex to maintain the double gap that is required. A second design, shown on the right in Figure 2.B.3, has a single 100 Ω cable connected between the 50 Ω generator and the 200 Ω antenna. The effect of this is that there are two impedance discontinuities, which reduce the total voltage incident upon the antenna feed arms by 11%. However, we believe that the smaller apex geometry may still result in a higher radiated field. Both reflector IRAs can be configured with either impedance matching network, so we can experiment with two identical antennas in either configuration. We also plan to compare configurations with and without feed-arm terminations.

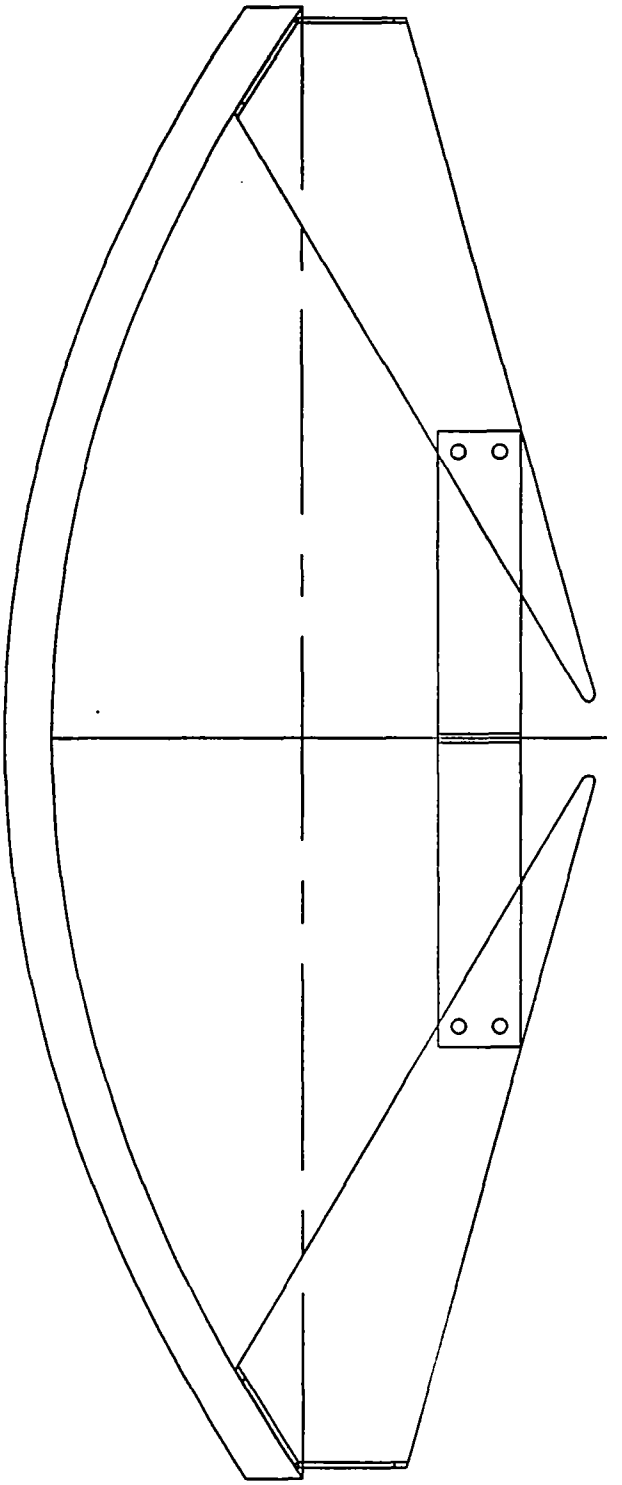

Figure 2.B.1. Reflector IRA, side view.

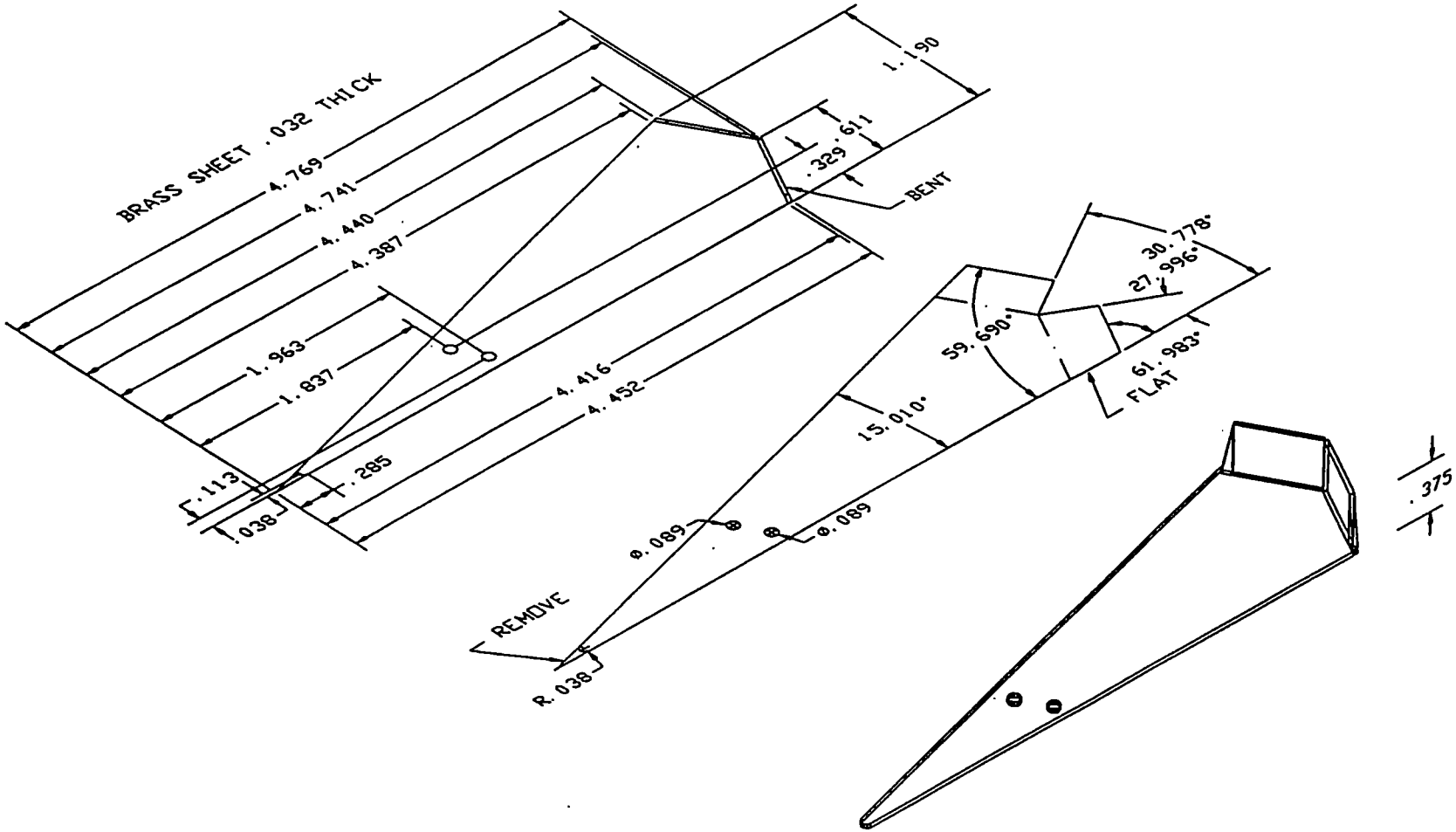

Figure 2.B.2. Reflector IRA feed arm sheet metal layout.

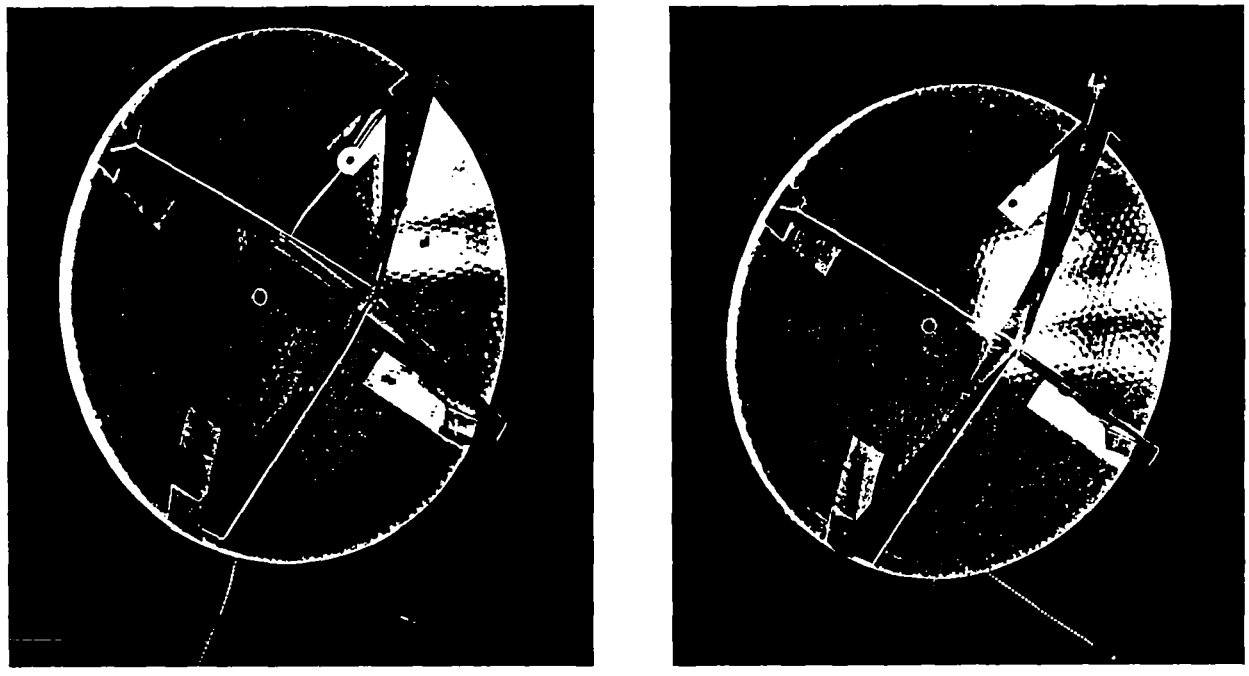

Figure 2.B.3. The reflector IRAs as built, showing two impedance matching networks. The standard balun, with two 100 Ω cables, is on the left. The modified impedance transformer using a single 100 Ω cable is on the right.

C. Reflector IRA Radiated Field on Boresight

Let us consider the fields that will be radiated by the reflector IRA on boresight. Recall that a single pair of feed arms has an impedance of 400 Ω, and two orthogonal pairs of arms are used. The reflector has an *F/D* of 0.3778, with a diameter of 9 inches, or 22.9 cm. The antenna is driven with an integrated-Gaussian step function, with a derivative risetime (final value divided by peak derivative) of t_d = 50 ps and peak voltage V_o into the 50 Ω balun feed cable. The methods used for calculating the radiated field are the same as those used in [2].

The radiated field $E(t)$ on boresight at a distance r is shown in Figure 2.C.1. Note that the plot is normalized to the peak step voltage V_o into the 50 Ω section of the balun feed. The theory used here takes into account the voltage amplification of the balun, as well as the effect of the second pair of arms. This correction was described earlier in [2, Section 5].

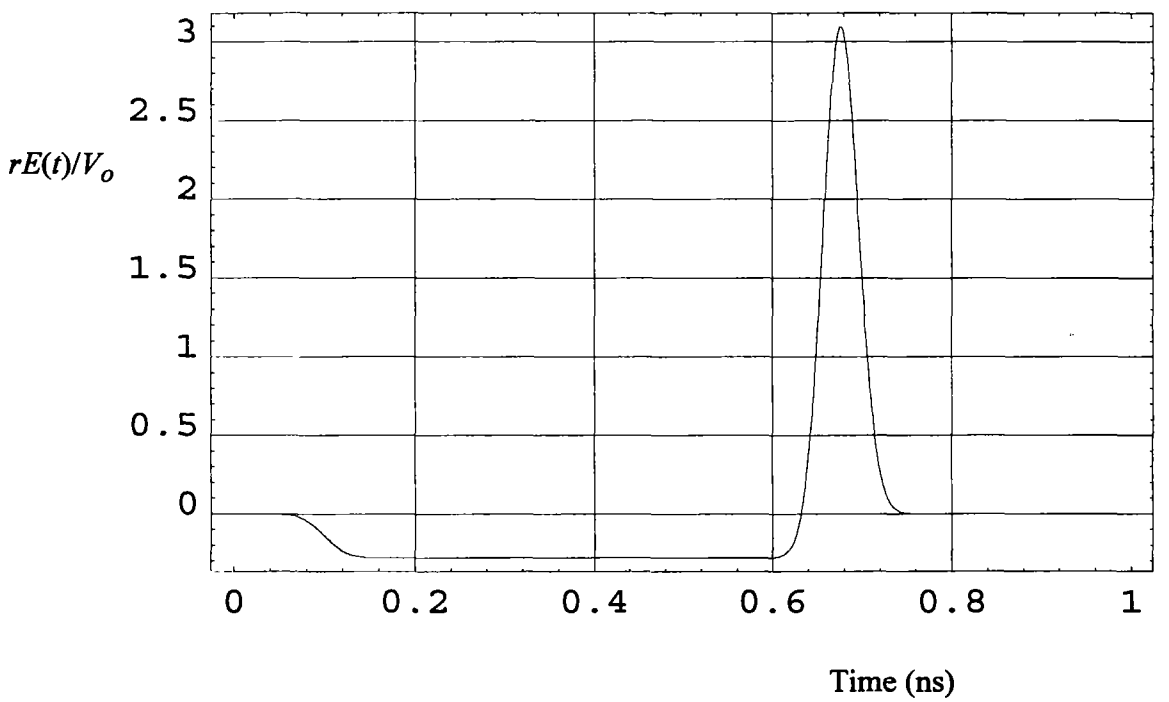

Figure 2.C.1. Radiated Field for the reflector IRA to be built

To calculate the received voltage after the signal passes through two identical reflector IRAs, we can predict that response with the theory of [2]. The result is shown in Figure 2.C.2. The two antennas are assume to be in each other's far field, using the same driving voltage as before. The received voltage is normalized to V_o/r. where r is the distance between the antennas.

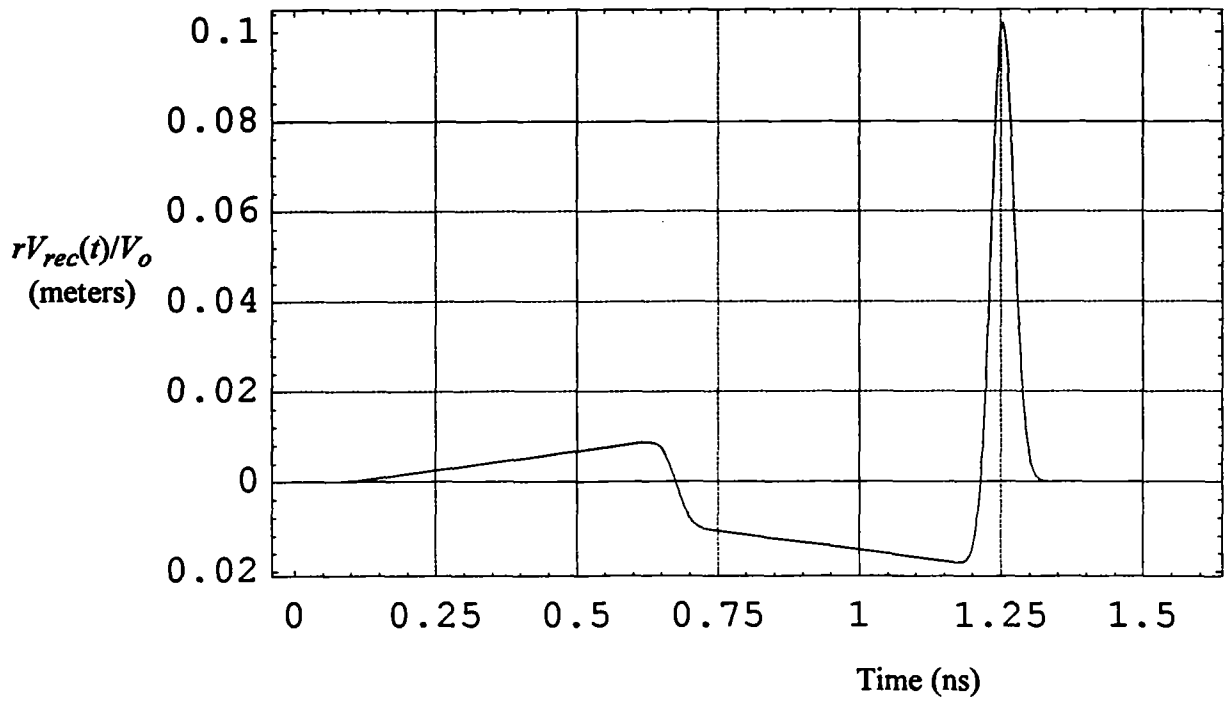

Figure 2.C.2. Received voltage for two reflector IRAs on boresight.

D. Reflector IRA Radiated Field Off-Boresight

We next consider how the fast part of the waveform varies as a function of angle. The theory was developed in considerable detail in [3], for the case of round conical feed arms. Although we have in this case flat-plate feed arms, we can use the theory for round conical arms of the same impedance as a good approximation. The theory of [3] was developed for only two feed arms, however, and we have four arms in the current design. Thus, some extension of that work is required.

When the conical geometry is projected onto a plane, we have an aperture field that is created from four conductors, as shown in Figure 2.D.1. The potential function is calculated by adding the potential for two two-wire problems, including translation. The potential function for a single pair of wires, where the charge centers are located at (x=0, y/a = 1), is

$$w_2(\zeta) \;=\; 2j\,\mathrm{arccot}(\zeta/a) \;=\; \ln\left(\frac{\zeta - ja}{\zeta + ja}\right) \qquad (2.D.1)$$

where a is the aperture radius. Here, $\zeta = x + jy$ is the location in the Cartesian coordinate space. This potential function is plotted in [3, Figure 2], so there is no need to repeat it here. The complex potential for the four-wire case is just a sum of two two-wire potentials that have been shifted and resized, i.e.,

$$w_4(\zeta) \;=\; w_2\left((z+\sqrt{2})/\sqrt{2}\right) \;+\; w_2\left((z-\sqrt{2})/\sqrt{2}\right) \qquad (2.D.2)$$

This function is complex, i.e., has both real and imaginary parts. Let us therefore set

$$u(\zeta) \;=\; \mathrm{Re}(w_4(\zeta)) \;,\qquad v(\zeta) \;=\; \mathrm{Im}(w_4(\zeta)) \qquad (2.D.3)$$

We can plot contours of constant u and v, and these are shown in Figure 2.D.2, for the upper right quadrant. The conductors correspond to a contour of constant u.

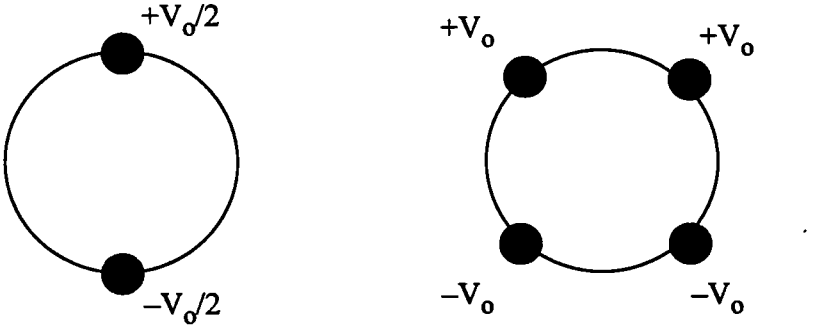

Figure 2.D.1. The apertures for a two-wire and four-wire configuration.

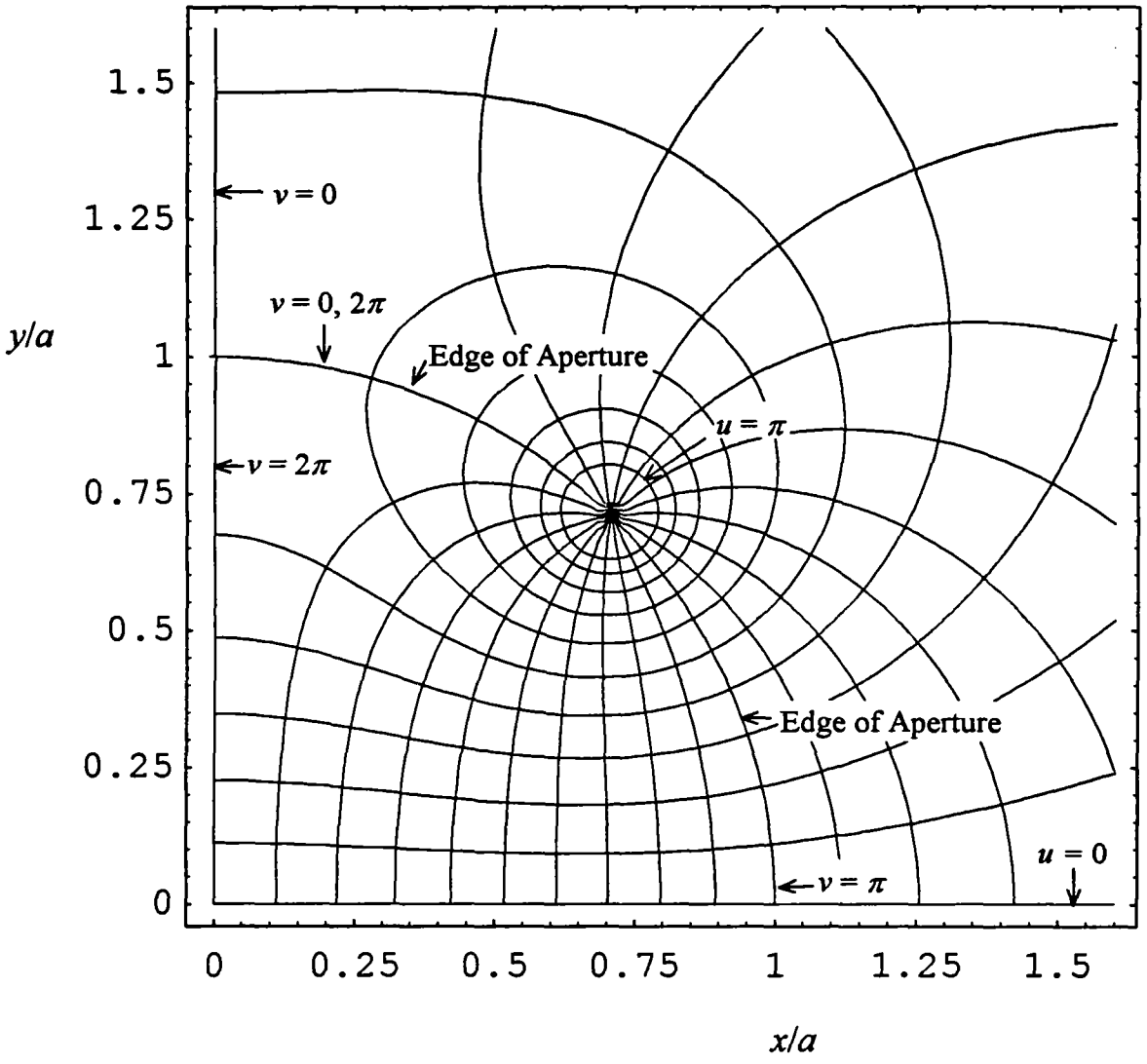

Figure 2.D.2. Contour map for $w_4(\zeta)$. Increments for u and v are $\pi/10$.

To calculate the radiated field, we need the aperture fields and the normalized aperture potentials. The aperture field, as usual, is

$$E_y(x,y) = \frac{-(2V_o)}{\Delta u}\frac{\partial u(x,y)}{\partial y} \tag{2.D.4}$$

where $2V_0$ is the voltage between the top and bottom conductors, and Δu is the change in u between the two conductors.

The normalized potentials are integrals over linear paths in the aperture field. We need to calculate these because the radiated field is proportional to them. The normalized potentials for the H-plane calculation is

$$\Phi^{(h)}(x) = -\frac{1}{(2V_o)}\int_{C_1(x)} E_y \, dy \tag{2.D.5}$$

where the contour $C_1(x)$ is a vertical line cut through the aperture plane, as shown in Figure 2.D.3. To simplify this H-plane integral, one merely substitutes (2.D.4) into (2.D.5), generating

$$\Phi^{(h)}(x) = \frac{1}{\Delta u}\int_{C_1(x)} \frac{\partial u}{\partial y} dy = \frac{2}{\Delta u}\, u\left(x, \sqrt{a^2 - x^2}\right) \tag{2.D.6}$$

We can now calculate $u(x,y)$ as the real part of the potential function given in (2.D.2). Note that the value of $u(x,y)$ is a maximum when it cuts through the conductors. At this point, the value of $u(x,y)$ is $u_o = \pi f_g$. where f_g is the relative impedance for a single pair of arms located on opposite sides of the circle (typically 400 Ω/ 377 Ω). Note also that for values of x that cut through the conductors, the normalized potential is unity. This normalized potential function is plotted in Figure 2.D.4, for a few different values of f_g.

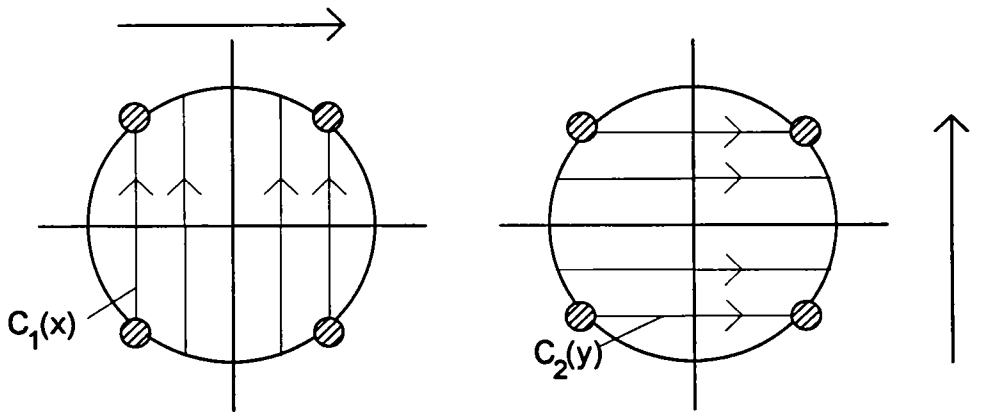

Figure 2.D.3. Locations of $C_1(x)$ and $C_2(y)$.

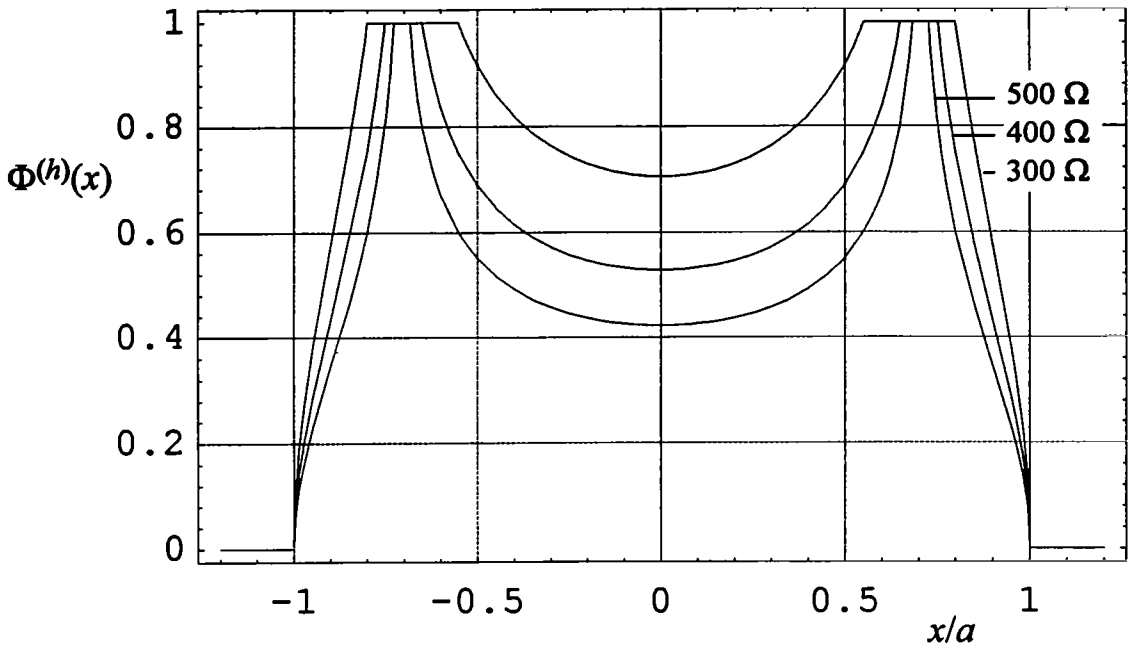

Figure 2.D.4. The normalized potential function $\Phi^{(h)}(x)$ for a few different impedances.

The normalized potential for the E-plane is expressed as

$$\Phi^{(e)}(y) = -\frac{1}{(2V_o)}\int_{C_2(y)} E_y\, dx = -\frac{1}{\Delta u}\int_{C_2(y)} \frac{\partial u}{\partial y}\, dx \qquad (2.D.7)$$

where $C_2(y)$ is a horizontal linear cut through the aperture plane, as shown in Figure 2.D.3. To evaluate this, we require the Cauchy-Riemann relation for analytic functions,

$$\frac{\partial u}{\partial y} = \frac{\partial v}{\partial x} \qquad (2.D.8)$$

which allows us to recast the integral as

$$\Phi^{(e)}(y) = \frac{-2}{\Delta u}\left[v\left(\sqrt{a^2 - y^2}, y\right) - v(0, y)\right] \qquad (2.D.9)$$

This is a particularly simple form, because the edges of the circular aperture are also lines of constant v. Thus, the normalized potential is evaluated analytically as

$$\Phi^{(e)}(y) = \begin{cases} 1/f_g & |y|/a < 1/\sqrt{2} \\ 0 & \text{else} \end{cases} \tag{2.D.10}$$

Note that we show a very abrupt transition between the two values, but it is actually more smooth. This transition occurs as $C_2(y)$ passes through the two wires, and if the wire is thin, an abrupt transition is an excellent approximation. We have plotted the normalized potentials for a few impedances in Figure 2.D.5.

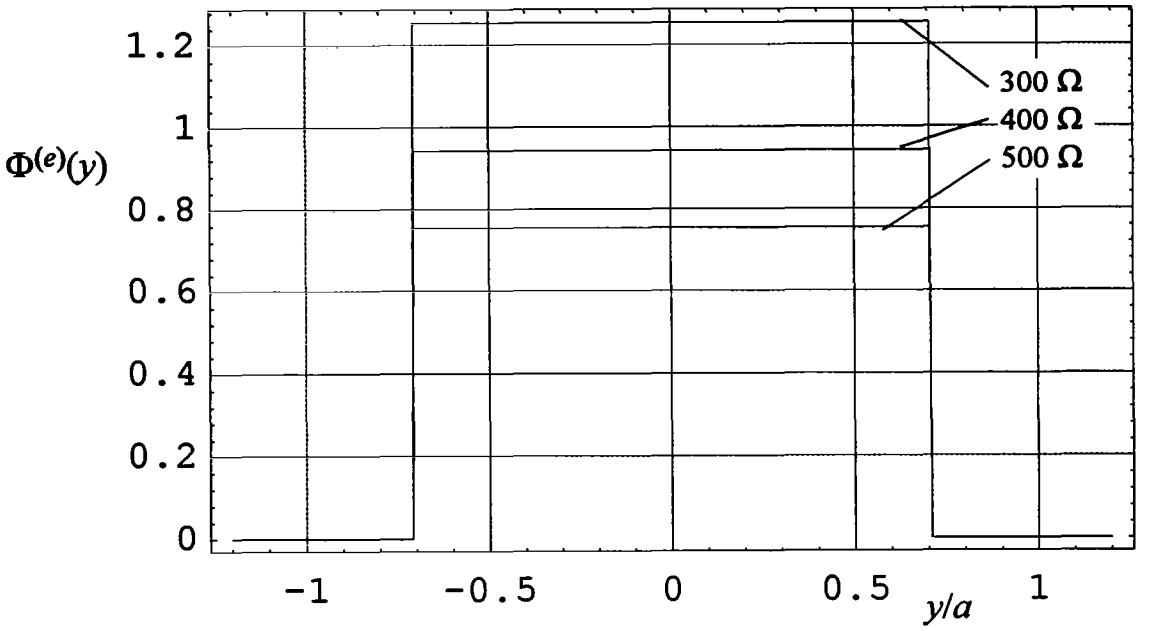

Figure 2.D.5. The normalized potential function $\Phi^{(e)}(y)$ for a few different impedances.

With the normalized potentials calculated, we can now calculate the radiated field as a function of angle off boresight in the H and E-planes. The H-plane and E-plane are the planes that are perpendicular and parallel to the dominant radiated field on boresight, respectively. In the H-plane and E-plane, the field radiated by a step voltage of magnitude $2V_o$ across the aperture is

$$\begin{aligned} \vec{E}_{step}^{(h)}(r,\theta,t) &= \vec{1}_y \left(\frac{-(2V_o)}{r}\right) \frac{\cot(\theta)}{2\pi} \Phi^{(h)}\left(\frac{ct}{a\sin(\theta)}\right) \\ \vec{E}_{step}^{(e)}(r,\theta,t) &= \pm \vec{1}_\theta \left(\frac{-(2V_o)}{r}\right) \frac{1}{2\pi\sin(\theta)} \Phi^{(e)}\left(\frac{ct}{a\sin(\theta)}\right) \end{aligned} \tag{2.D.11}$$

In Figure 2.D.6 we have plotted these for our case of diameter = 2 a = 22.9 cm. Time plots of these two step responses are shown for a few different values off-boresight in the H and E-planes. Note that we cannot plot the step response at 0°, because it is a delta function there, with infinite magnitude and zero width.

To obtain a radiated field, we convolve the step responses with the derivative of the driving voltage. To drive the antenna, we assume an integrated Gaussian with a peak magnitude of V_o and a risetime of t_d = 50 ps. Note that the effect of the balun is to double the voltage, generating a voltage drop across the aperture of (2 V_o). Thus, we are consistent with earlier calculations.

We have plotted the time response at θ = 0°, 2.5°, 5°, 10° and 20° away from boresight in the E and H planes, in Figure 2.D.7. Note that the H-plane response falls off more rapidly at wider angles, because the antenna aperture is more broad in the direction perpendicular to the H-plane (y direction) than perpendicular to the E-plane (x direction).

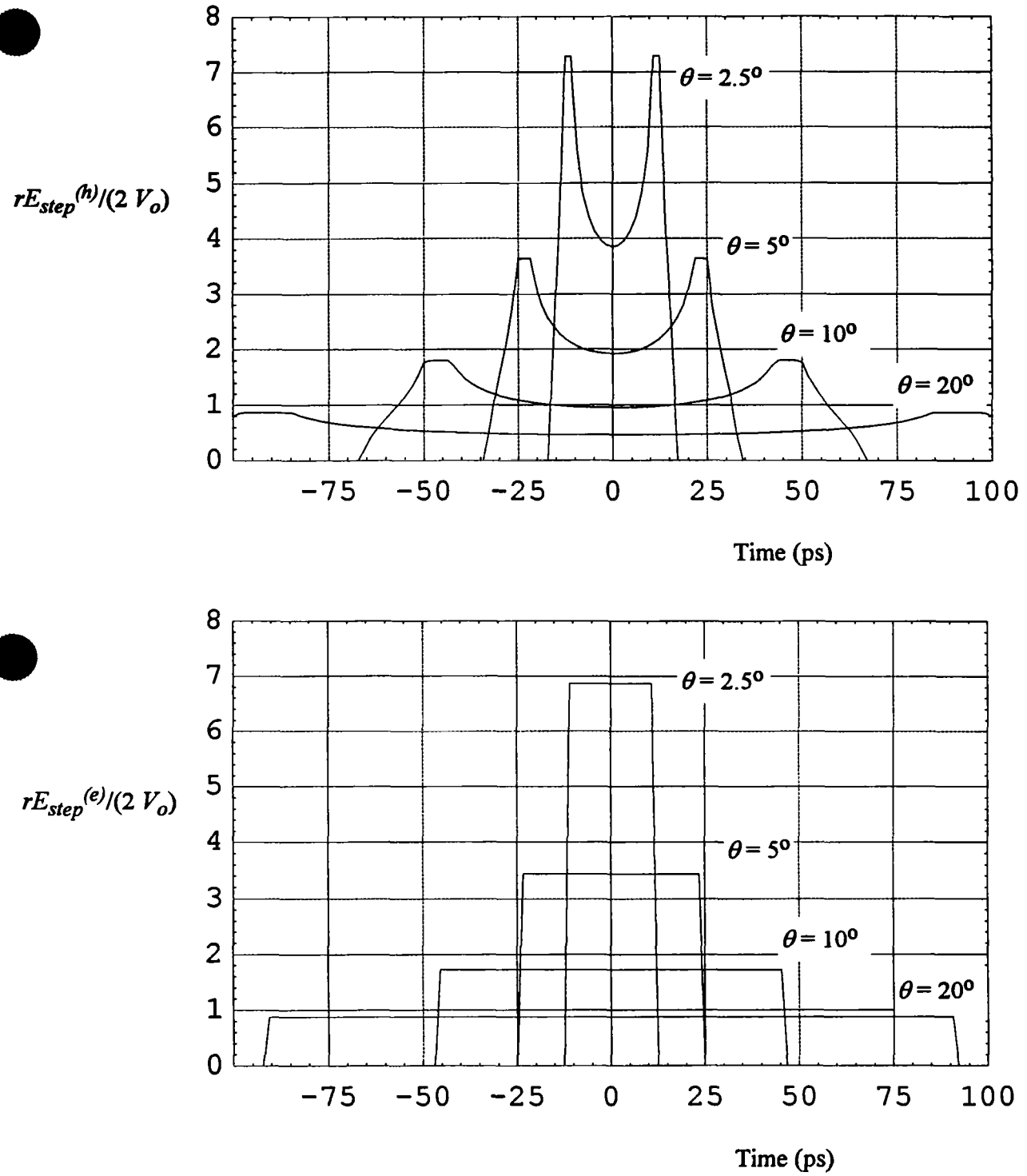

Figure 2.D.6. Step response of the 4-armed reflector IRA in the H-plane (top) and the E-plane (bottom).

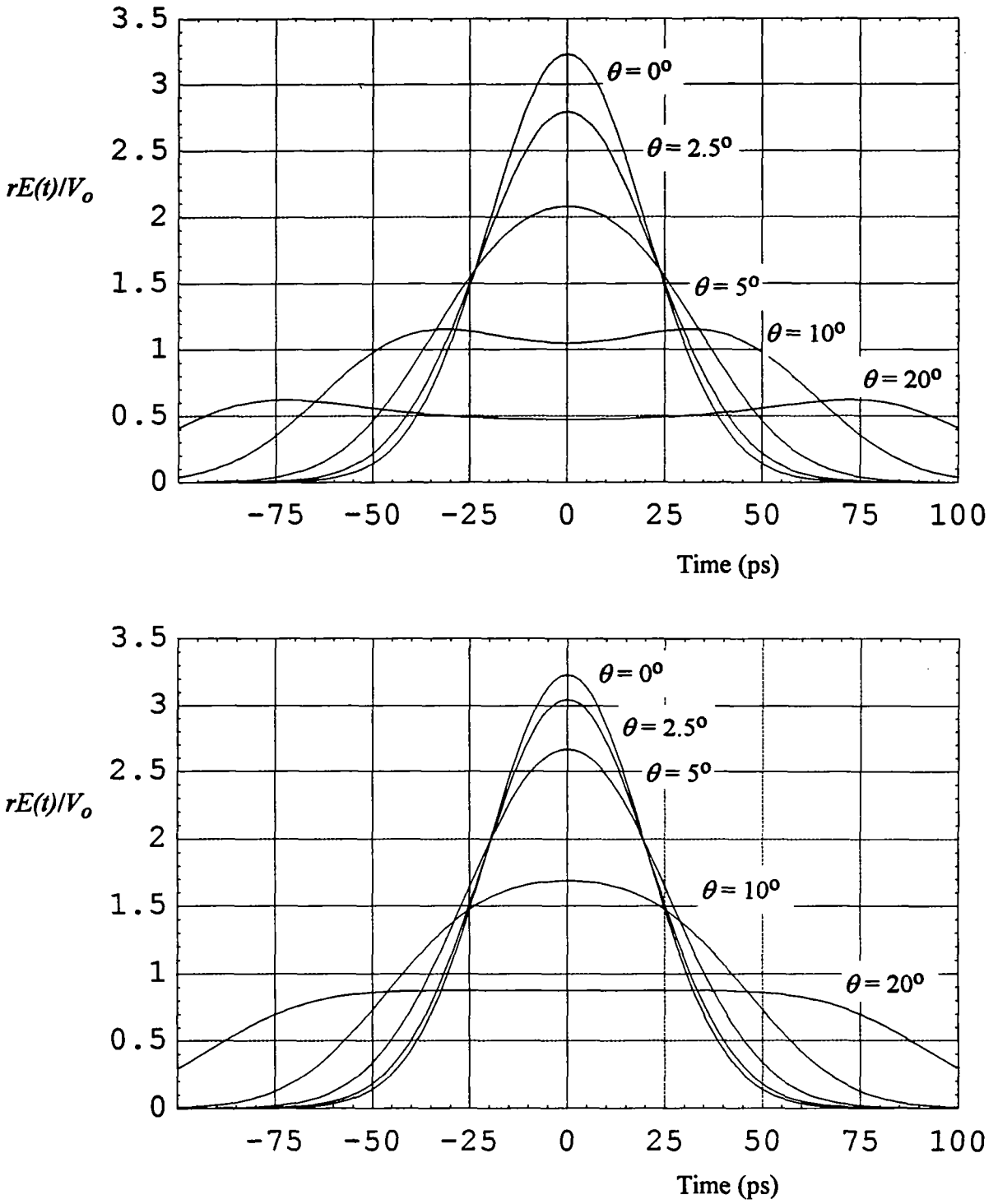

Figure 2.D.7. Fast part of the H-plane (top) and E-plane (bottom) radiated field for the reflector IRA.

E. Received Voltage for Reflector IRA

Next, we consider the received voltage when two identical reflector IRAs are used, one transmitting and one receiving. We furthermore assume that one of the antennas may be pointed at an angle off boresight, in either the E or H planes, as shown in Figure 2.E.1. This configuration is of interest because it will be used to make antenna pattern measurements.

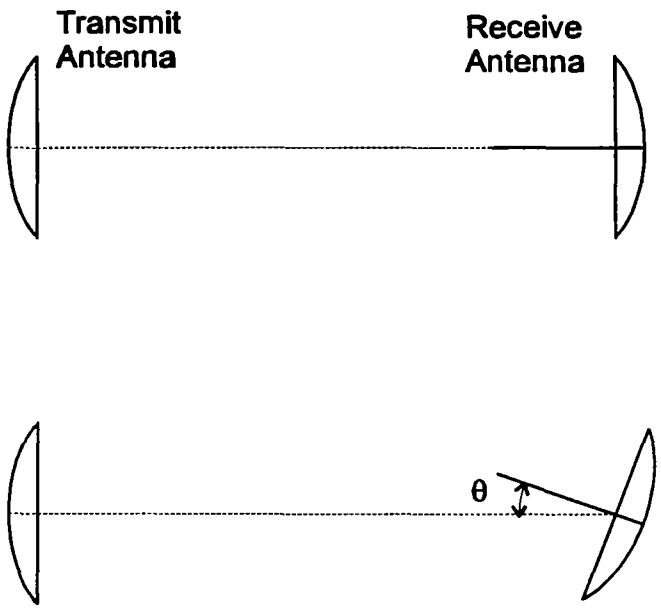

Figure 2.E.1. Configuration for antenna pattern measurements.

To make these predictions, we need an expression for $h(t)$ both on and off-boresight. Thus, we need to compare the fast portions of the radiated field, as calculated two different ways. The field radiated on boresight is just

$$\begin{aligned} E(r,t) &= \frac{1}{2\pi c f_g r} h(t) \circ \frac{2\,dV_{inc}(t)}{dt} \\ h(t) &= a\sqrt{2}\left[\delta_a(t-2F/c) - \frac{c}{2F}\left[u(t)-u(t-2F/c)\right]\right] \end{aligned} \tag{2.E.1}$$

where the feed impedance of a single pair of arms is expressed as f_g, where $f_g = Z_{feed}/Z_o$, and Z_o=376.727 Ω is the impedance of free space. Furthermore, a is the reflector radius, F is the focal length of the reflector, and r is the distance out the to the observer. In addition, $\delta_a(t)$ is an approximation to the Dirac delta function, $u(t)$ is the Heaviside step function and the "o" operator indicates a convolution. The incident voltage, V_{inc}, is the incident voltage onto the 50 Ω feed

line, and Z_{feed} as defined here refers to the impedance between two arms. Normally, Z_{feed} = 400Ω.

To obtain the off-boresight $h(t)$, we simply replace the delta function above with a smeared-out version of the delta function. To obtain the smeared-out version, we note that the fast portion of the radiated field on boresight is just

$$E_{step}(r,t) = \frac{2V_o}{r}\frac{a\sqrt{2}}{2\pi c f_g}\delta(t) \tag{2.E.2}$$

Furthermore, the off-boresight step responses in the H and E-planes are, from the previous section,

$$\begin{aligned}
\vec{E}_{step}{}^{(h)}(r,\theta,t) &= \vec{1}_y\left(\frac{(2V_o)}{r}\right)\frac{\cot(\theta)}{2\pi}\;\Phi^{(h)}\left(\frac{ct}{a\sin(\theta)}\right)\\
\vec{E}_{step}{}^{(e)}(r,\theta,t) &= \pm\vec{1}_\theta\left(\frac{(2V_o)}{r}\right)\frac{1}{2\pi\sin(\theta)}\;\Phi^{(e)}\left(\frac{ct}{a\sin(\theta)}\right)
\end{aligned} \tag{2.E.3}$$

where the normalized potential functions $\Phi^{(h)}(x)$ and $\Phi^{(e)}(y)$ are defined in section 2.D. Comparing the above two expressions, we find they are equivalent on boresight when we replace the delta function in (2.1) with a smeared-out delta function defined for both the H- and E-planes. These delta functions are just

$$\begin{aligned}
\delta^{(h)}(\theta,t) &= \frac{c f_g}{\sqrt{2}a}\cot(\theta)\;\Phi^{(h)}\left(\frac{ct}{a\sin(\theta)}\right)\\
\delta^{(e)}(\theta,t) &= \frac{c f_g}{\sqrt{2}a}\csc(\theta)\;\Phi^{(h)}\left(\frac{ct}{a\sin(\theta)}\right)
\end{aligned} \tag{2.E.4}$$

Thus, we find new expressions for the antenna step response, $h(t)$, in the H- and E-planes as

$$\begin{aligned}
h^{(h)}(t,\theta) &= a\sqrt{2}\left[\frac{c f_g}{\sqrt{2}a}\cot(\theta)\;\Phi^{(h)}\left(\frac{c(t-2F/c)}{a\sin(\theta)}\right) - \frac{c\cos(\theta)}{2F}[u(t)-u(t-2F/c)]\right]\\
h^{(e)}(t,\theta) &= a\sqrt{2}\left[\frac{c f_g}{\sqrt{2}a}\csc(\theta)\;\Phi^{(e)}\left(\frac{c(t-2F/c)}{a\sin(\theta)}\right) - \frac{c\cos(\theta)}{2F}[u(t)-u(t-2F/c)]\right]
\end{aligned} \tag{2.E.5}$$

These can now be used in the standard expressions for the radiated field. In general, for our problem, we will use the boresight expression for the transmit antenna and the above off-boresight expressions for the receive antenna.

We can now calculate the received voltage as

$$V^{(h)}_{rec}(t,\theta) = \frac{1}{2\pi c f_g r} h(t) \circ h^{(h)}(t,\theta) \circ \frac{dV_{inc}(t)}{dt}$$
$$V^{(e)}_{rec}(t,\theta) = \frac{1}{2\pi c f_g r} h(t) \circ h^{(e)}(t,\theta) \circ \frac{dV_{inc}(t)}{dt} \qquad \text{(2.E.6)}$$

We have calculated these for a few angles off-boresight in Figures 2.E.2 and 2.E.3.

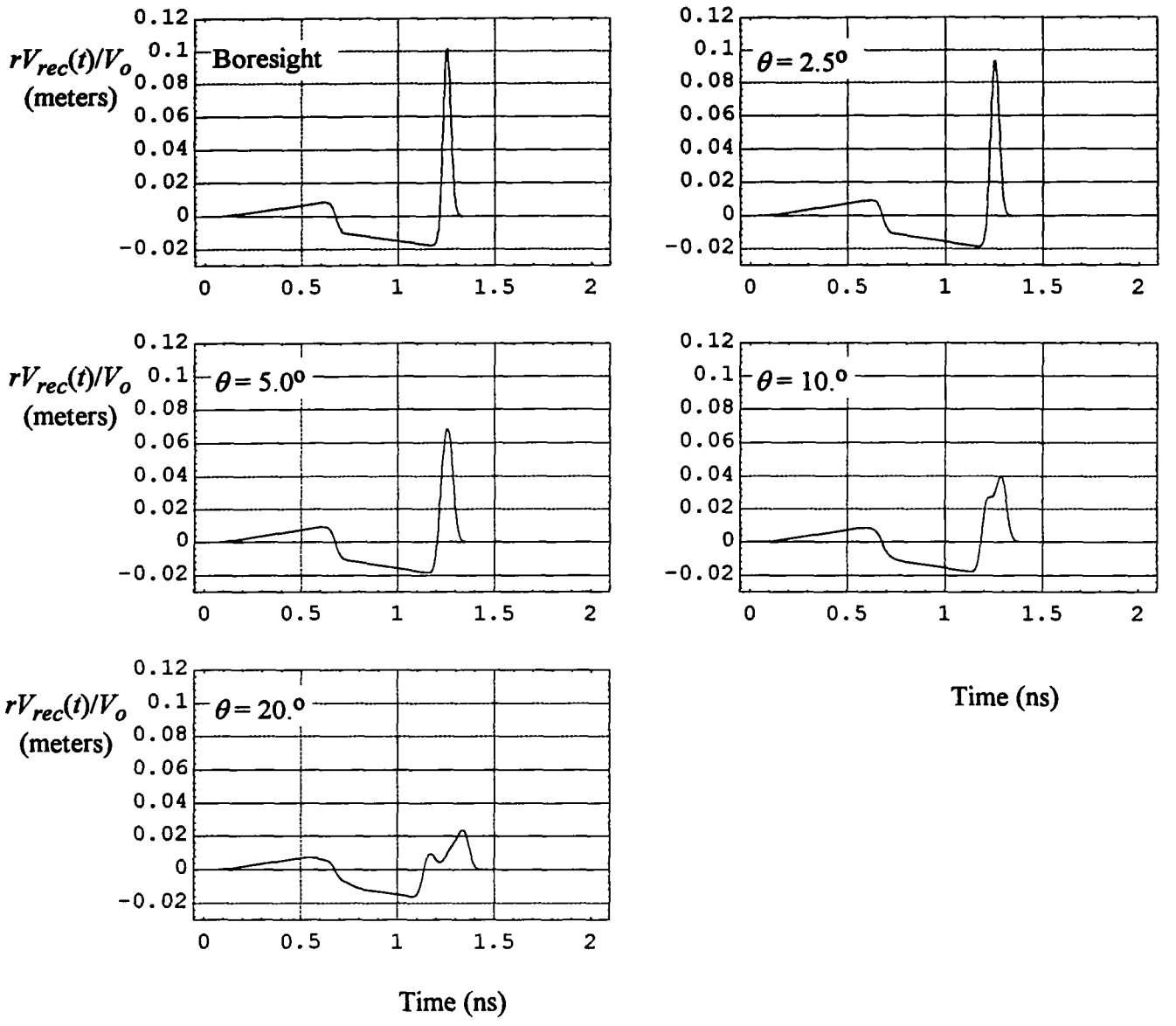

Figure 2.E.2. Received voltage in the H-plane for the reflector IRA, with two identical antennas.

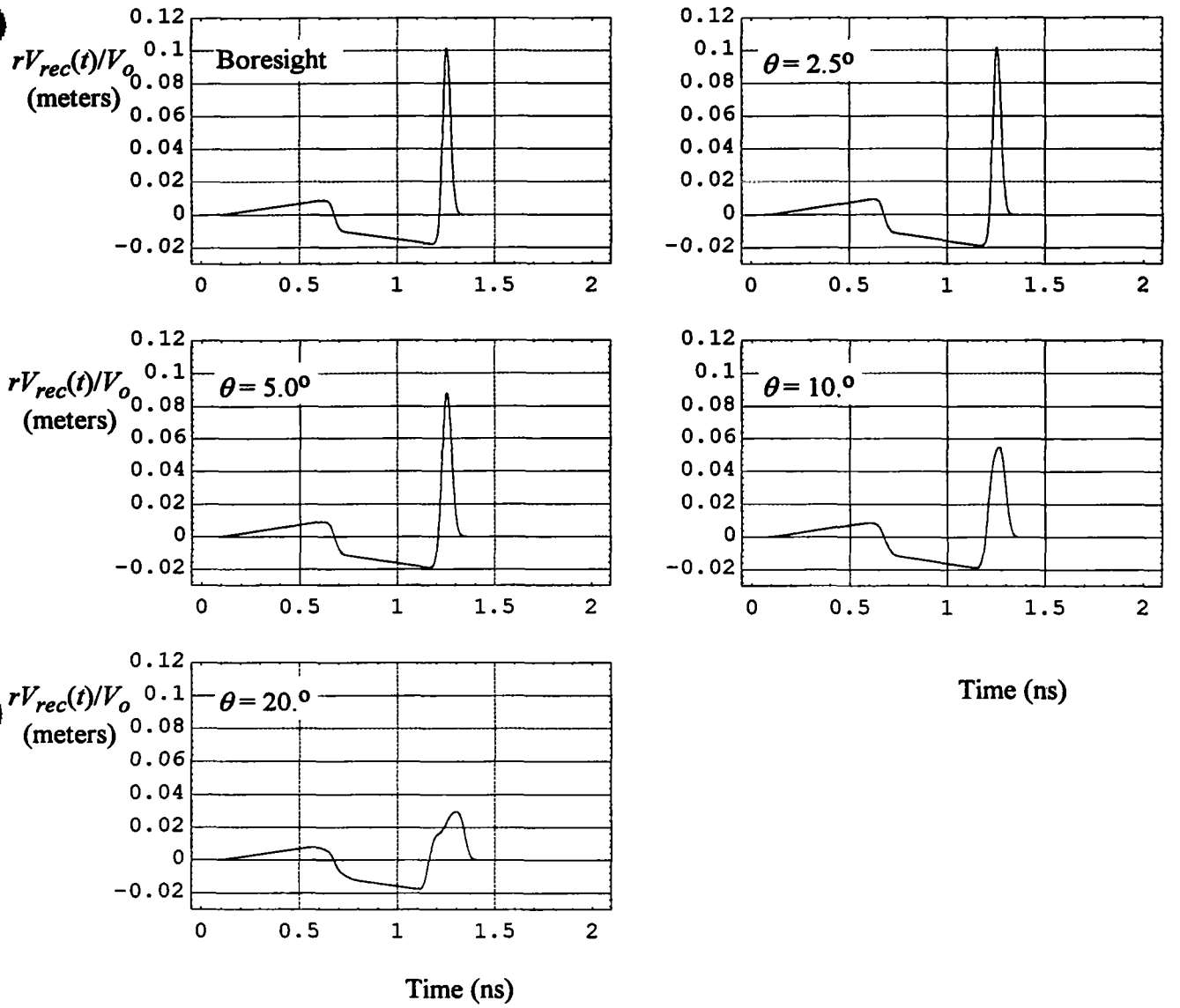

Figure 2.E.3. Received voltage in the E-plane for the reflector IRA, with two identical antennas..

III. Lens IRA

A. Design Equations

A sketch of the solid dielectric IRA is shown in Figure 3.A.1. The antenna was built from high-density polyethylene, which has a dielectric constant of 2.31. The lens in front will convert the spherical wave to a plane wave in the aperture, which is suitable for high-gain radiation. We investigate here the shape of that lens.

The interface is an ellipse of revolution, as described in [4, Section 3]. A diagram of the relevant parameters is shown in Figure 3.A.2, which shows a sketch of the lens through a radial slice. Note that in cylindrical coordinates, we denote the radial coordinate as Ψ, where many other authors use ρ. We do so in order to avoid a possible conflict in meaning of ρ to indicate charge.

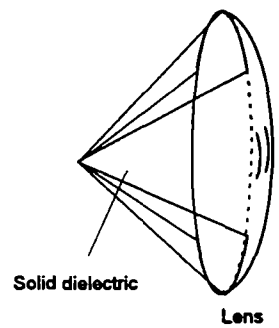

Figure 3.A.1. A solid dielectric lens IRA.

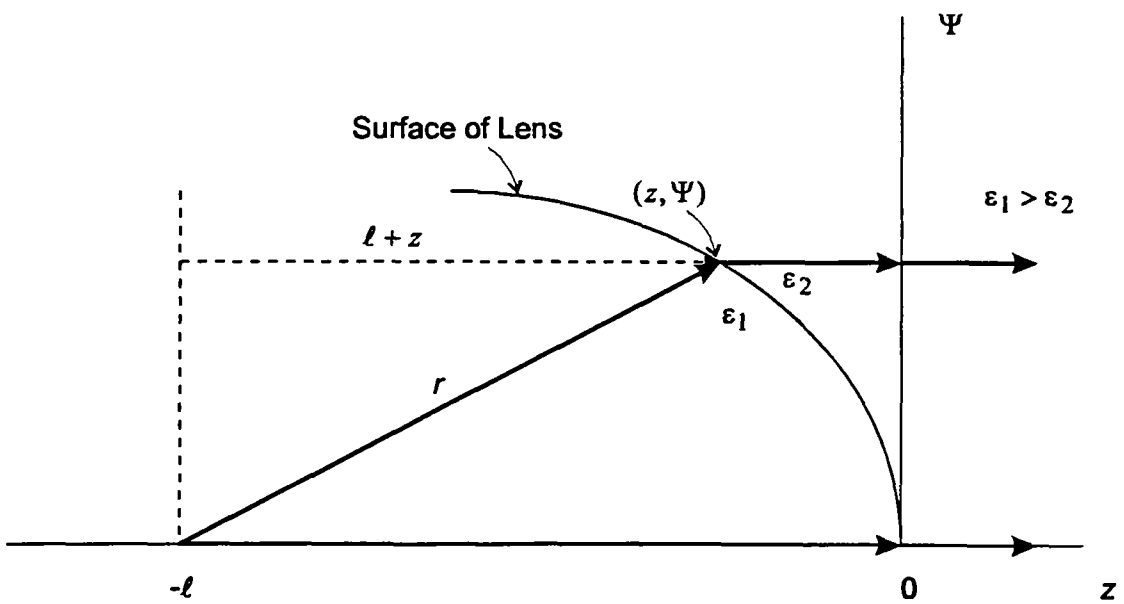

Figure 3.A.2 Elliptical interface for converting a plane wave to spherical wave.

Let us derive now the equations that define the surface. In the Ψ–z plane the equation of the surface is derived from transit-time considerations as

$$\begin{aligned} \sqrt{\varepsilon_1}\ell &= \sqrt{\varepsilon_1}r + \sqrt{\varepsilon_2}(-z) \\ \sqrt{\varepsilon_1}(\ell - r) &= \sqrt{\varepsilon_2}(-z) \end{aligned} \tag{3.A.1}$$

We further expand r in its z and Ψ components as

$$r^2 = (\ell + z)^2 + \Psi^2 \tag{3.A.2}$$

Combining the above equations, and making the substitutions

$$\begin{aligned} \varepsilon_r &= \varepsilon_1 / \varepsilon_2 \\ q &= \sqrt{\frac{\varepsilon_2}{\varepsilon_1}} = 1/\sqrt{\varepsilon_r} \end{aligned} \tag{3.A.3}$$

we find

$$(\ell + z)^2 + \Psi^2 = (\ell + qz)^2 \tag{3.A.4}$$

This is the equation to be solved.

Continuing from the above equations, we can simplify the description of the surface still further. With some rearrangement, including completing the square, we find

$$\begin{aligned} \frac{\Psi^2}{1-q^2} + z^2 + \frac{2\ell}{1+q}z &= 0 \\ \frac{\Psi^2}{1-q^2} + \left(z + \frac{\ell}{1+q}\right)^2 &= \frac{\ell^2}{(1+q)^2} \end{aligned} \tag{3.A.5}$$

If we now make the substitutions

$$\begin{aligned} a &= \frac{\ell}{1+q} = \frac{\ell}{1+1/\sqrt{\varepsilon_r}} \\ b &= \ell\sqrt{\frac{1-q}{1+q}} = \ell\sqrt{\frac{\sqrt{\varepsilon_r}-1}{\sqrt{\varepsilon_r}+1}} \\ \frac{b}{a} &= \sqrt{1-\frac{1}{\varepsilon_r}} \end{aligned} \tag{3.A.6}$$

we arrive at the final equation

$$\frac{(z+a)^2}{a^2} + \frac{\Psi^2}{b^2} = 1 \tag{3.A.7}$$

This surface is immediately recognizable as a simple ellipse with major axes of a and b, and offset in the z' direction by $-a$.

Note that all rays in the first medium originate at one of the focuses of the ellipse. To prove this, we note that the distance from the center of the ellipse to its focus is given by [5]

$$\begin{aligned} d^2 &= a^2 - b^2 \\ d &= \pm\frac{\ell q}{1+q} = \pm\frac{\ell}{\sqrt{\varepsilon_r}+1} \end{aligned} \tag{3.A.8}$$

Note that we have indicated the focal distance by d instead of c, to avoid a conflict with the symbol for the speed of light. The focus is located at a distance of $(a + d) = \ell$ from the interface, thus proving that the rays originate at a focus of the ellipse.

Note also that when there is a reflection from the interface, it reflects back toward the other focus. This property can be used to "smear" out reflections from the surface that can bounce off the source and re-radiate. The idea here is that late reflections should be damped out.

Let us now consider the error in time delay that is incurred when the prolate spheroid is approximated by a sphere. A diagram of the spherical approximation to the ellipse is shown n Figure 3.A.3. There is a certain maximum radius Ψ_{max} that we wish to allow. To see where the prolate spheroid intersects the maximum radius, we consider the equation of the ellipse. The value of $z = z_p$ corresponding to the maximum radius is

$$\begin{aligned} \frac{(z+a)^2}{a^2} + \frac{\Psi^2}{b^2} &= 1 \\ z_p &= -a + a\sqrt{1 - \frac{\Psi_{max}^2}{b^2}} \end{aligned} \tag{3.A.9}$$

As an example, we assume $\varepsilon_r = 4$ and $\ell = 26.25$ cm, and $\Psi_{max} = 11.25$ cm. From (3.A.6) we find $a = 17.5$ cm, $b = 15.16$ cm, $c = 8.75$ cm, so $z_p = -5.77$ cm.

Next, we identify where the maximum radius intersects the sphere, from the equation of the circle. The equation for the circle is

$$\frac{(z+\ell)^2}{\ell^2} + \frac{\Psi^2}{\ell^2} = 1$$

$$z_s = -\ell + \sqrt{\ell^2 - \Psi_{\max}{}^2} \tag{3.A.10}$$

Continuing our example, we find $z_s = -2.53$ cm. The error in time delay is calculated using the error in path length, $z_e = z_p - z_s$, corrected by the error in square root of the dielectric constant along this path, $\sqrt{\varepsilon_r} - 1$, which should have been air instead of dielectric. The electric path error is therefore

$$t_e = \frac{\sqrt{\varepsilon_r} - 1}{c}(z_s - z_p) \tag{3.A.11}$$

In our example, this works out to 108 ps. This is probably too large a time difference if the goal is a 50 ps Full Width Half Max (FWHM) radiated impulse.

Under what circumstances, then, will the spherical approximation be valid? While it is difficult to summarize for all cases, in general, the spherical approximation improves for smaller Ψ_{max}/b and for larger ε_r.

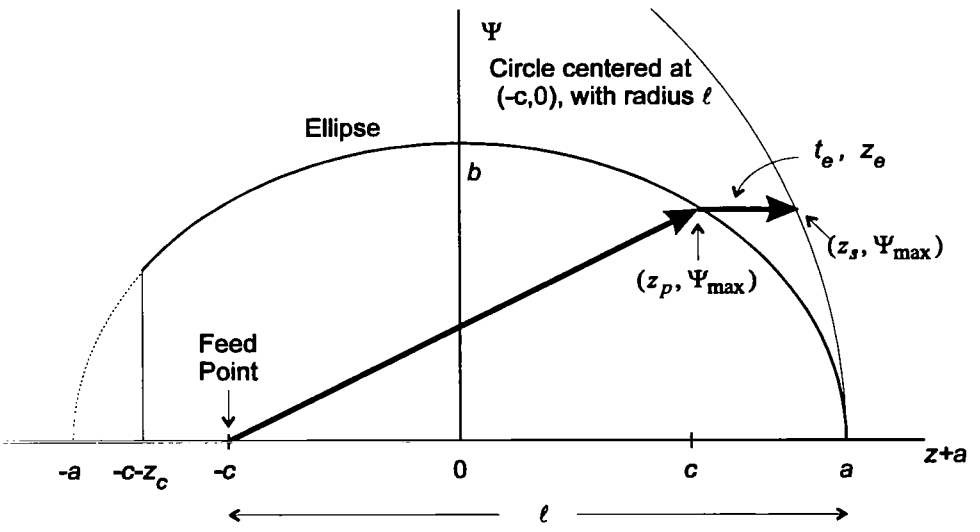

Figure 3.A.3. Spherical approximation to the ellipse.

B. Construction Details for the Lens IRA

The Lens IRA was built from a high-density polyethylene, whose dielectric constant was specified by the manufacturer to be 2.31. Although we had considered lexan (a polycarbonate), it was impossible to verify its propagation properties at the frequencies of interest.

The dimensions for the lens IRA are shown in Figure 3.B.1. From the diagram, we find

ε_r	= 2.31	
ℓ	= 11.0 in	= 27.94 cm
ℓ_1	= 7.39 in	= 18.77 cm
a	= 6.63 in	= 16.84 cm
b	= 5.00 in	= 12.70 cm
d	= 4.35 in	= 11.06 cm
x_{max}	= 3.61 in	= 9.17 cm
y_{max}	= 4.45 in	= 11.30 cm

where all of the above symbols refer to Figure 3.B.2. The final design of the lens IRA is shown in Figures 3.B.3 - 3.B.6

Figure 3.B.7 shows the completed dielectric immersed lens IRA ready for testing. The design gives us the flexibility to optimize the impedance taper of the TEM expansion section and to move the point source location for optimum focus. This is accomplished by removing covers which surround the point source. In addition, the design provides for changing the impedance of the transmission line transformer section, if desired, and installing a 50 Ω input cable for initial TDR measurements.

Figure 3.B.8 shows the component parts of the solid dielectric lens IRA. All plastic parts are made of low density polyethylene to maintain a uniform dielectric constant. The parts listed from left to right are as follows:

1. coaxial transmission line matching section with nickel-zinc Ferrite isolator cores and connector.
2. upper and lower covers with mounting screws and nuts.
3. lens cone assembly with attached mounting fixture and polyethylene through bolts.
4. triangular copper TEM tapered transmission line electrodes.

The lens has a prolate spheroidal surface which is difficult to machine accurately. Accuracy of the aspheric surface was a primary concern, since any deviation from the design shape degrades the radiated pulse risetime. The ideal calculated surface was compared to the measured surface. The actual surface was measured using analog dial gauges with an accuracy of 0.076 mm (0.003 in) . The maximum deviation from ideal is 1.6 mm (0.062 in.) for the first lens and 1.2 mm (0.046 in) for the second lens. The RMS deviation is 0.28 mm (0.011 in) for the first

lens, and 0.41 mm (0.016 in) for the second lens. These numbers are both well below our RMS deviation specification of 0.5 mm (0.02 in). For polyethylene, with a dielectric constant of 2.31 and index of refraction of 1.51, the deviation from ideal should lead to a risetime degradation of less than 10 ps, which is sufficient for our purposes.

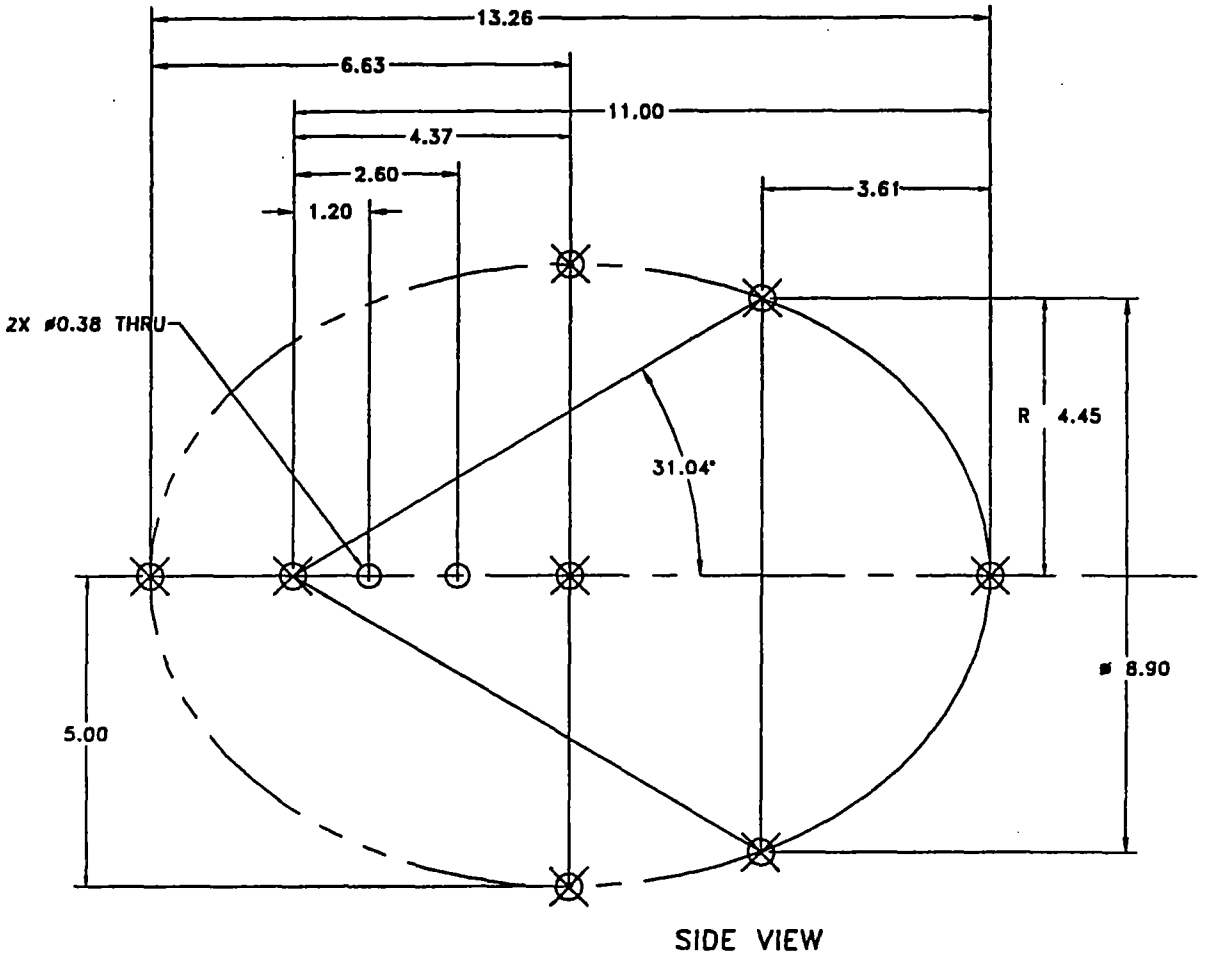

Figure 3.B.1. Sketch of the lens IRA.

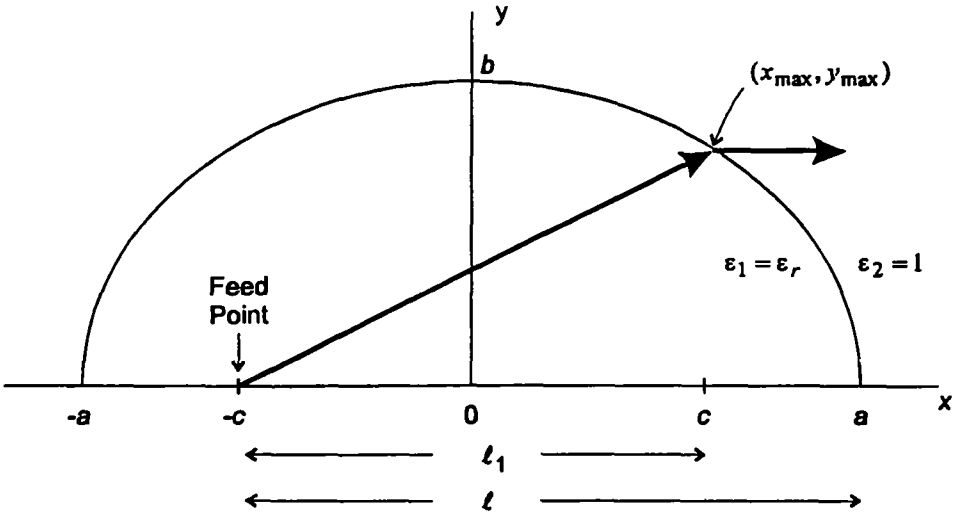

Figure 3.B.2. The prolate spheroid lens.

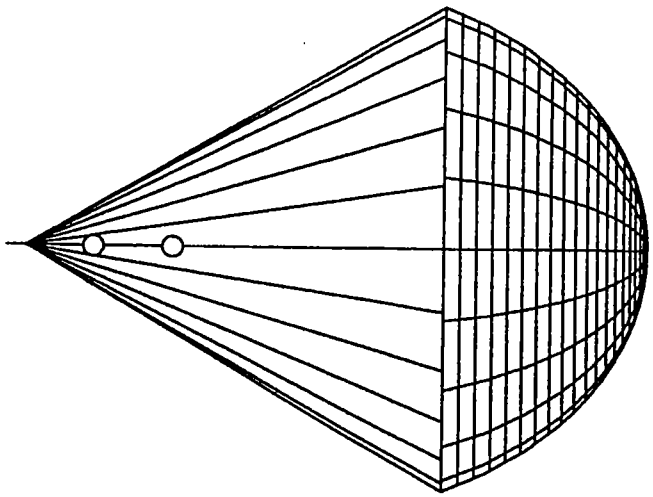

Figure 3.B.3. Lens cone assembly.

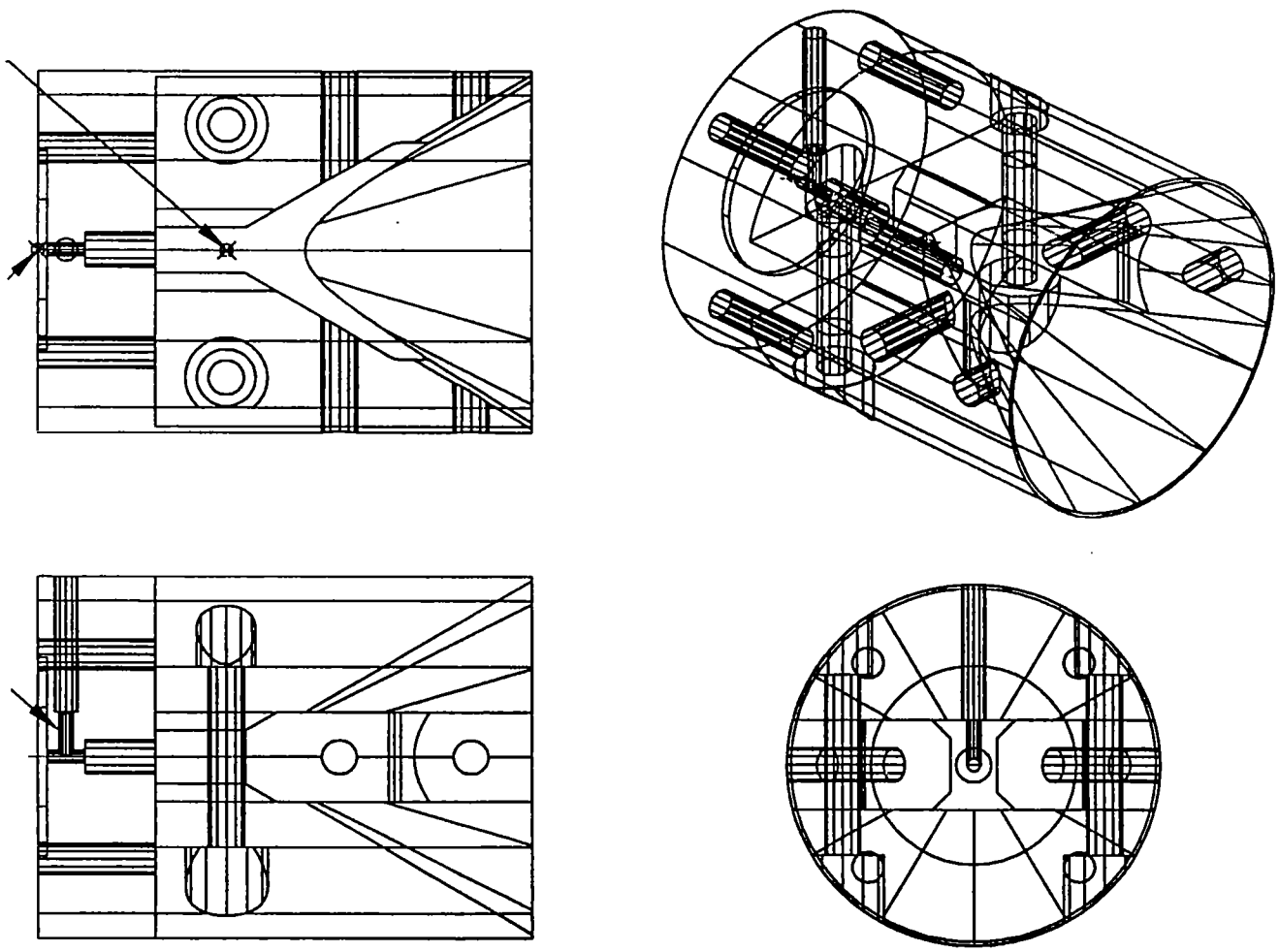

Figure 3.B.4. Details of the tailpiece.

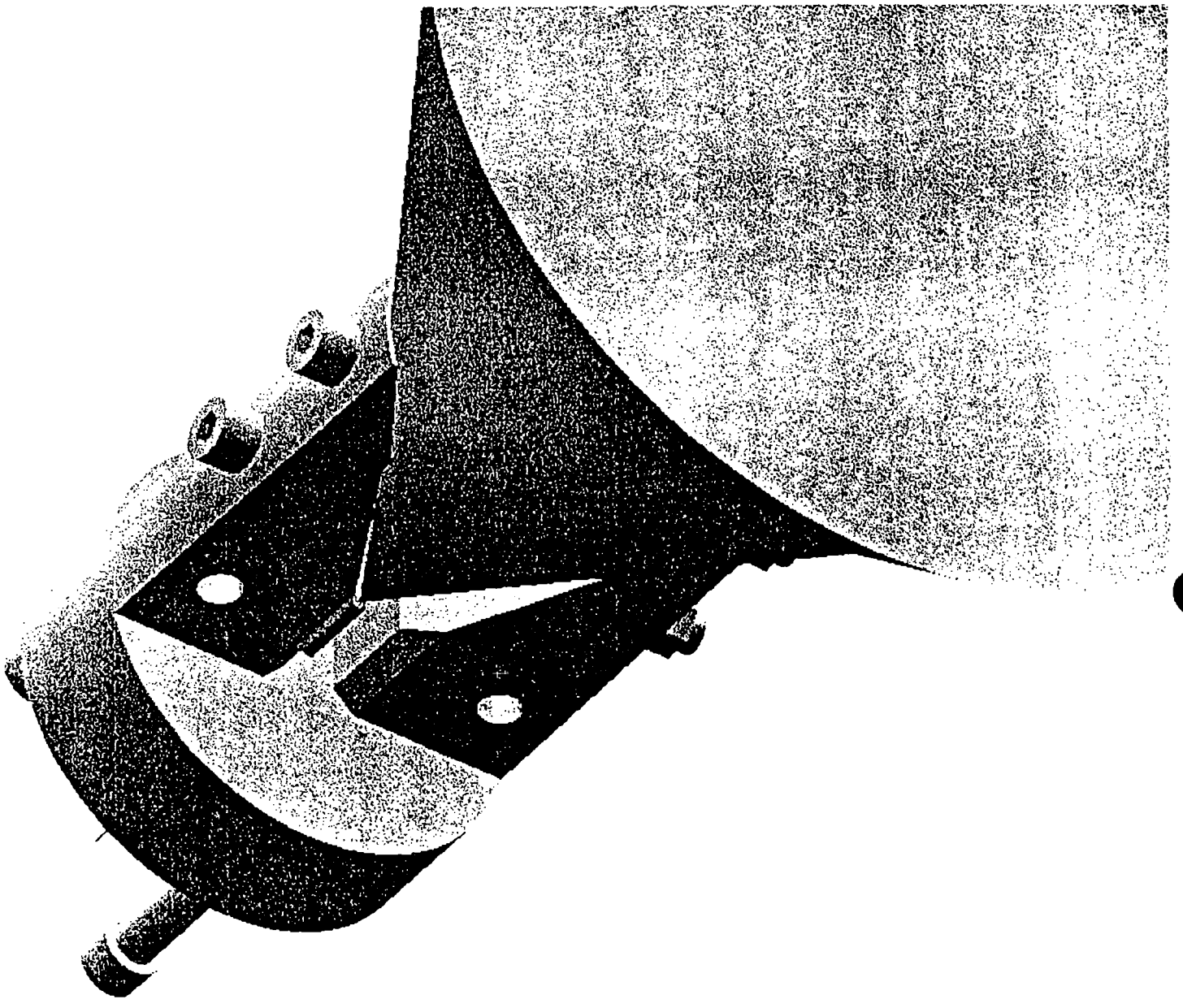

Figure 3.B.5. Lens IRA with top and bottom mount covers removed.

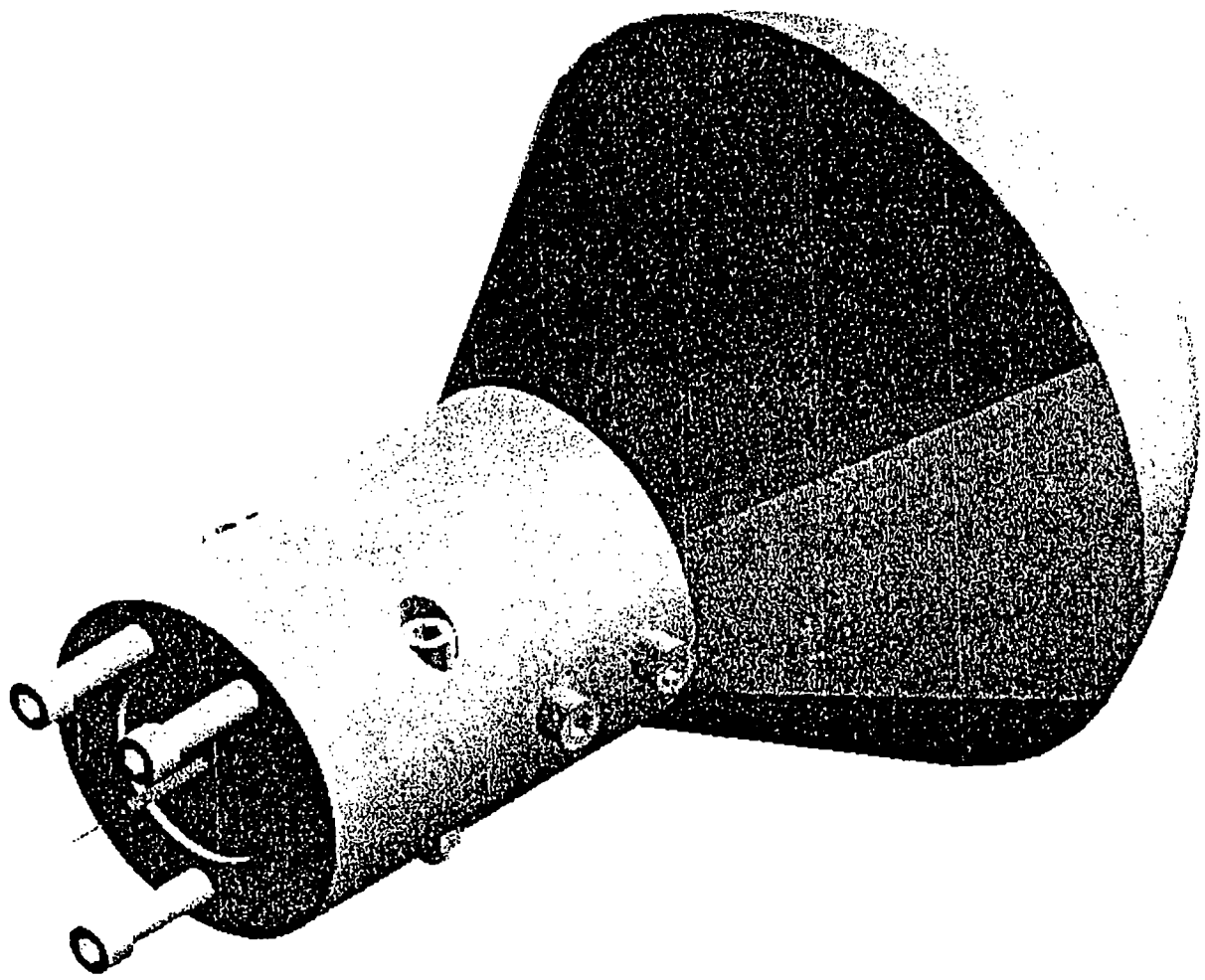

Figure 3.B.6. Lens-cover assembly, fully assembled.

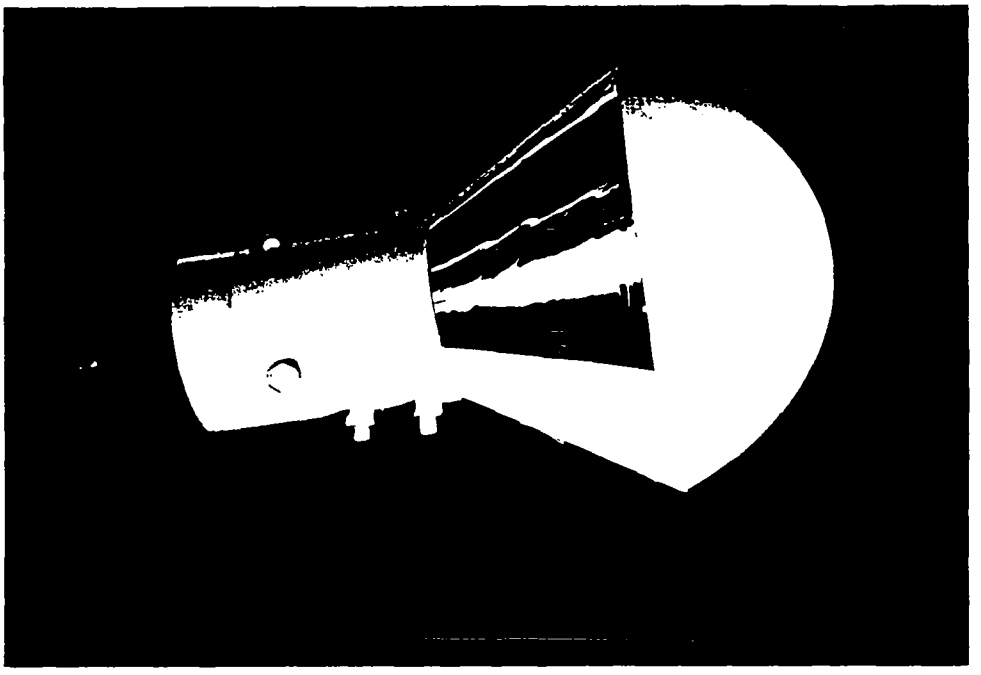

Figure 3.B.7. Completed 9-inch diameter solid dielectric lens IRA, ready for testing

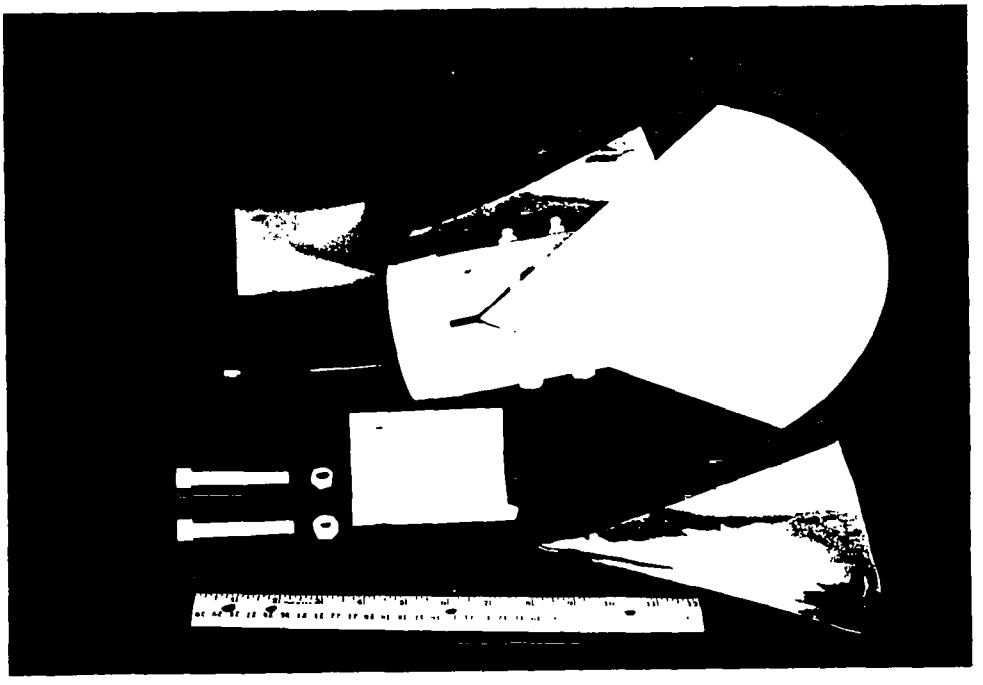

Figure 3.B.8. Component parts for the 9-inch diameter solid dielectric lens IRA

C. Lens IRA Radiated Field on Boresight

Let us next consider the radiated field on boresight for the lens IRA. We use the theory of [2] with a $t_d = 50$ ps integrated Gaussian driving function.

$$E(r,t) = \frac{h_a\,\tau}{2\pi c f_g\, r}\left[\frac{dV(t)}{dt} - \frac{c}{2\ell_1\sqrt{\varepsilon_r}}\left[V(t) - V(t - 2\ell_1\sqrt{\varepsilon_r}/c)\right]\right] \qquad (3.C.1)$$

$$\tau = \frac{2}{1+\sqrt{\varepsilon_r}} \equiv \text{air-to-dielectric transmission coefficient}$$

where ℓ is the length of the horn out to the end of the lens, r is the distance out to the observer, and h_a is an effective height function that depends upon feed impedance (f_g). Note that $f_g = Z_{feed}/Z_o$ refers to the normalized impedance of the feed *embedded* in the dielectric material. For optimal radiation, $Z_{feed} \times \sqrt{\varepsilon_r} = Z_o/2 = 377/2\ \Omega$. At this feed impedance, each arm of the TEM horn has an angular width of 90 degrees, and $h_a \sim 0.85 \times$ radius of aperture.

Because of the dielectric material, we have included two modifications to the above radiated field that are not normally included. First, we have modified the round-trip transit time, $c/2\ell_1\sqrt{\varepsilon_r}$, to include the dielectric. Second, we have adjusted the leading coefficient by a factor of τ, the air-to-dielectric transmission coefficient. (It should be pointed out that the above transmission coefficient is different from that used in [2]). To clarify the calculation of the transmission coefficient, let us extend the conductors beyond the end of the dielectric, as shown in Figure 2.1. We know that the field radiated from the extended aperture (in air) is

$$E(r,t) = \frac{h_a}{2\pi c f_{g2}\, r}\frac{dV_2(t)}{dt} \qquad (3.C.2)$$

Furthermore, the various parameters in the aperture extension can be related to the corresponding parameters in the dielectric as

$$V_2 = V_1\frac{2}{1+1/\sqrt{\varepsilon_r}}, \qquad f_{g2} = \sqrt{\varepsilon_r} f_{g1} \qquad (3.C.3)$$

where the subscript 1 refers to quantities embedded in the dielectric, and the subscript 2 refers to quantities in the extended aperture. The voltages are related by the dielectric-to-air transmission coefficient. Substituting (3.C.3) into (3.C.2), we find

$$E(r,t) = \frac{h_a\,\tau}{2\pi c f_{g1}\, r}\frac{dV_1(t)}{dt}, \qquad \tau = \frac{2}{1+\sqrt{\varepsilon_r}} \qquad (3.C.4)$$

This is in exactly the same form as (3.C.1), noting that V_1 and f_{g1} refer to the quantities in the dielectric. Note also that τ is just the transmission coefficient from air to dielectric.

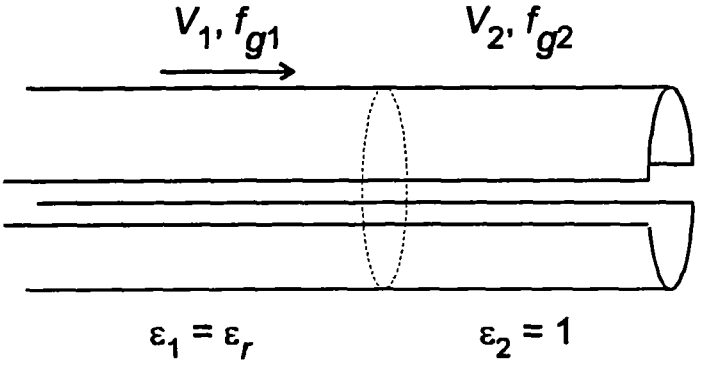

Figure 3.C.1. Extended aperture for calculating the field radiated from a solid dielectric lens IRA.

For clarity, we derive the receive mode characteristics. If the aperture were in air, the received voltage would be

$$V_{rec}(t) = h_a E_{inc}(t) \tag{3.C.5}$$

Since the antenna is embedded in dielectric, the received voltage must be adjust by the air-to-dielectric voltage transmission coefficient. Thus, we have

$$V_{rec}(t) = h_a \tau E_{inc}(t) \quad , \qquad \tau = \frac{2}{1+\sqrt{\varepsilon_r}} \tag{3.C.6}$$

Thus, we see that the net effect of embedding the antenna is to replace $h(t)$ with $\tau h(t)$, where $h(t)$ is the impulse response in reception or the normalized step response in transmission. Note that implied in the above rule is that the round-trip transit time must also be adjusted.

Finally, we note that in (3.C.1) we have expressed the radiated field in terms of the voltage launched onto the antenna. This is somewhat unusual, since we would normally express the radiated field in terms of a port voltage. We used the antenna voltage because we expect to experiment with the impedance taper (from 50 Ω to about 124 Ω). It is unclear exactly how this taper will be built, so we will add this feature to our model when we decide the ultimate form of the transition.

Thus, we drive the antenna with a t_d = 50 ps smoothed step. The radiated field on boresight is shown in Figure 3.C.2, normalized to V_o/r, where V_o is the peak voltage on the antenna. The received voltage after passing through two identical lens IRAs is predicted using the theory of [2], and is plotted in Figure 3.C.3.

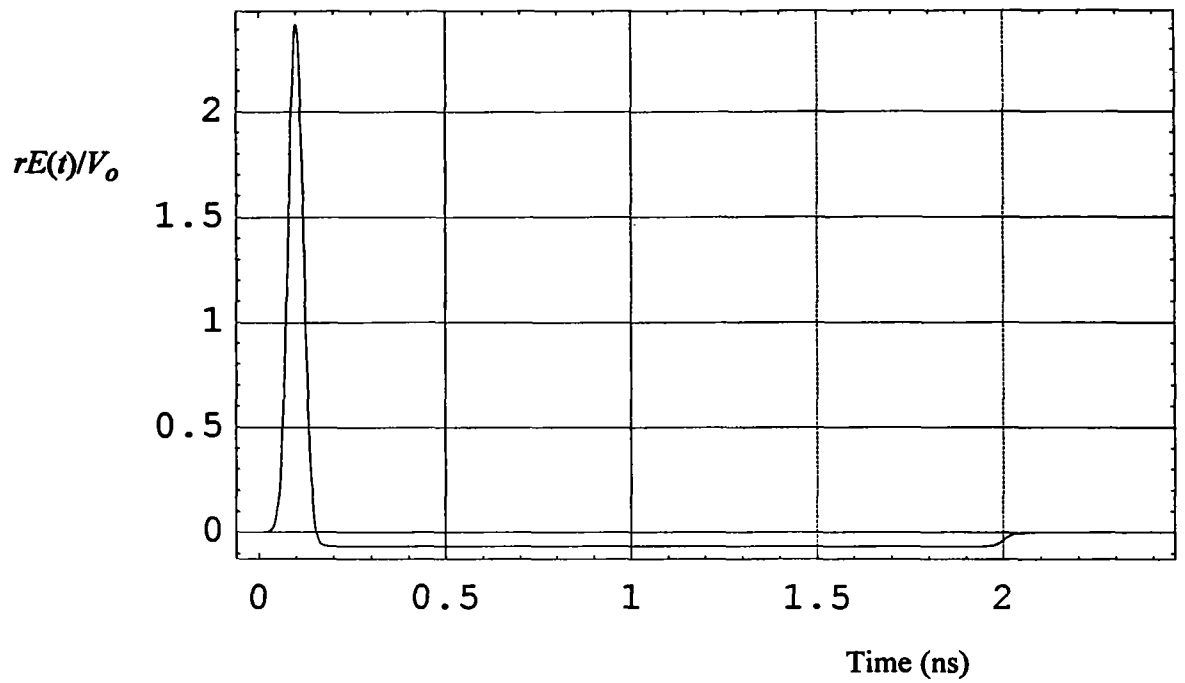

Figure 3.C.2. Radiated Field for the lens IRA.

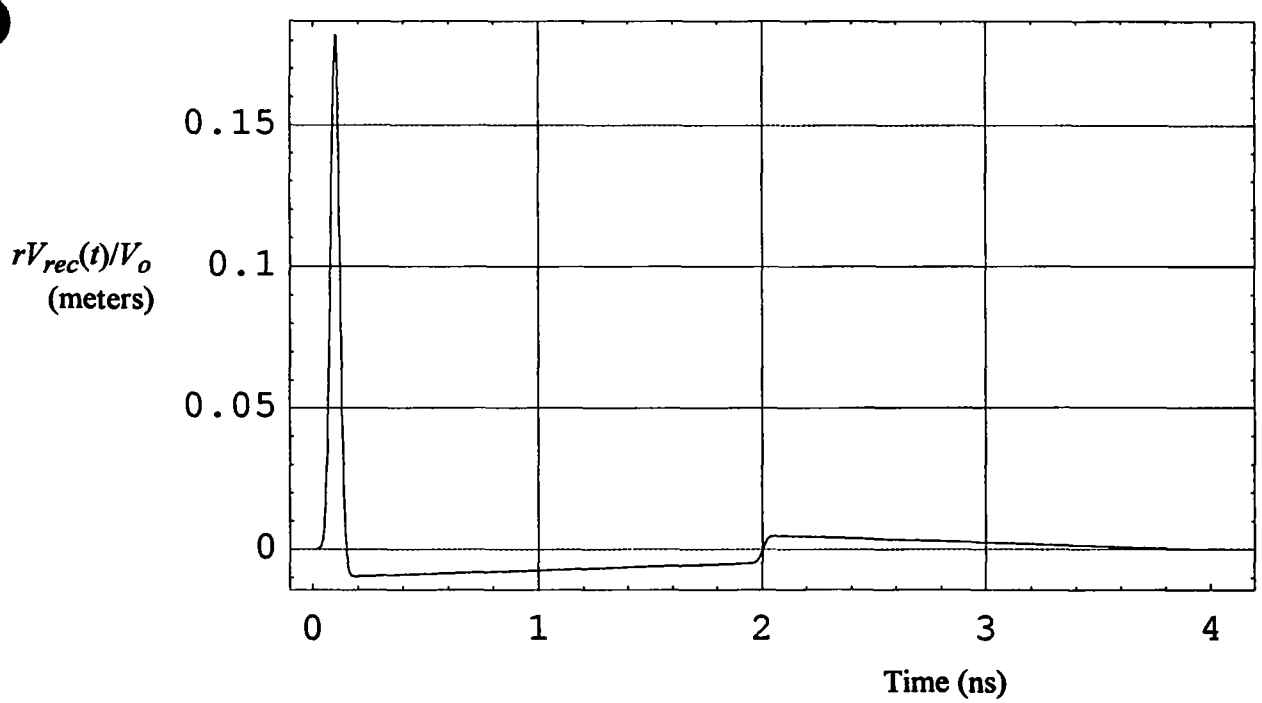

Figure 3.C.3. Received voltage for two lens IRAs on boresight.

D. Lens IRA Radiated Field Off-Boresight

Let us now consider how the fast part of the waveform varies as a function of angle. The theory was developed in [6] for an air-filled aperture, using an approximation to the normalized potential. The development in [6] was a linear approximation of a theory that was worked out in [3]. In this note we use the exact potential function, and we correct for the dielectric material. The aperture is shown in Figure 3.D.1.

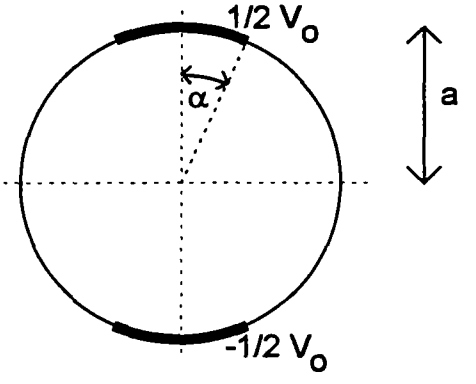

Figure 3.D.1. The geometry for curved plates, two-arm and four-arm configurations.

The first step in the procedure is to establish an aperture field as a derivative of a complex potential. The potential function we use is

$$w = \operatorname{arcsn}\left[\frac{1}{j\,m^{1/4}}\frac{z/a-1}{z/a+1}\right], \qquad \frac{z}{a} = \frac{1+j\,m^{1/4}\operatorname{sn}(w|m)}{1-j\,m^{1/4}\operatorname{sn}(w|m)} \tag{3.D.1}$$

where sn($w|m$) is one of the Jacobi elliptic functions, and arcsn is its inverse. The relationship between m and α is

$$\tan(\alpha) = \frac{1-m^{1/2}}{2m^{1/4}}, \qquad m = \left[\frac{1-\sin(\alpha)}{\cos(\alpha)}\right]^4 \tag{3.D.2}$$

The characteristic impedance of the configuration is $Z_c = Z_o f_g$, where

$$f_g = \frac{K(m)}{K(m_1)} \tag{3.D.3}$$

In this equation, $K(m)$ is the complete elliptic integral, and $m_1 = 1-m$.

The radiated field is calculated in a manner analogous to the equivalent calculation with the reflector IRA in Section 2.D. The only difference is a different aperture field, which changes the normalized potentials, $\Phi^{(h)}(x)$ and $\Phi^{(e)}(y)$. To clarify, the aperture field is

$$E_y(x,y) = \frac{-V_o}{\Delta u}\frac{\partial u(x,y)}{\partial y} \tag{3.D.4}$$

where V_0 is the voltage between the top and bottom conductors, and Δu is the change in u between the two conductors. The normalized potentials are

$$\begin{aligned} \Phi^{(h)}(x) &= -\frac{1}{V_o}\int_{C_1(x)} E_y\, dy = \frac{2}{\Delta u}u\left(x, \sqrt{a^2-x^2}\right) \\ \Phi^{(e)}(y) &= -\frac{1}{V_o}\int_{C_2(y)} E_y\, dx = -\frac{1}{\Delta u}\int_{C_2(y)}\frac{\partial u}{\partial y}\,dx \end{aligned} \tag{3.D.5}$$

where the contours $C_1(x)$ and $C_2(y)$ are as shown in Figure 3.D.2. Due to symmetry considerations, when $\alpha = 45^0$, $\Phi^{(h)}(x) = \Phi^{(e)}(y)$. Since that is the case of interest here, we only have to calculate $\Phi^{(h)}(x)$. Note that for values of x that cut through the conductors, the normalized potential is unity. This normalized potential function is plotted in Figure 3.D.3 for $f_g = 0.5$ in air

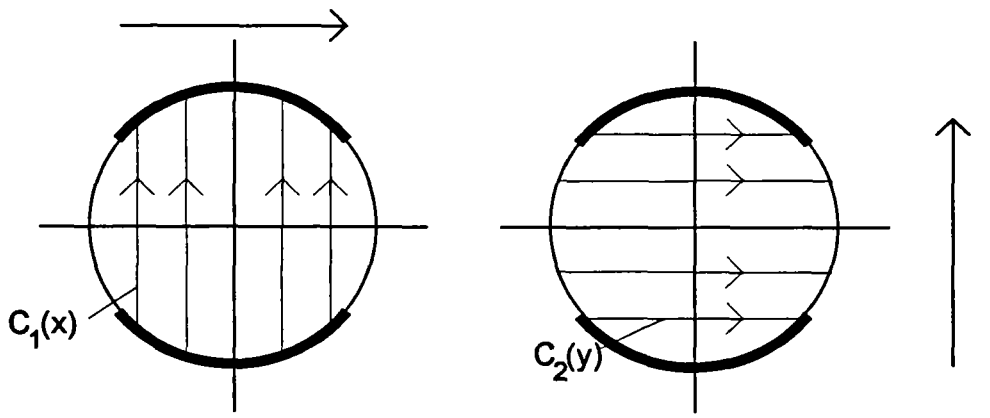

Figure 3.D.2 Locations of $C_1(x)$ and $C_2(y)$.

With the normalized potentials calculated, we can now calculate the radiated field as a function of angle off boresight in the H and E-planes. The field radiated by a step voltage of magnitude V_o across the aperture is

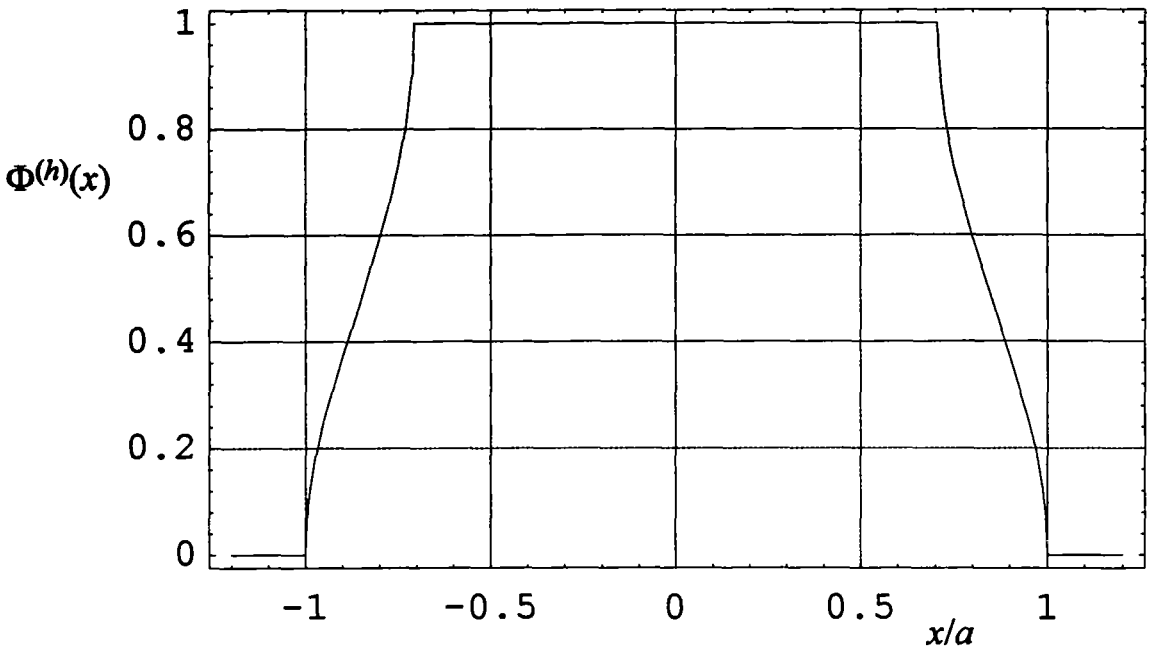

Figure 3.D.3. The normalized potential function $\Phi^{(h)}(x)$ for f_g. = 0.5.

$$\vec{E}_{step}{}^{(h)}(r,\theta,t) = \vec{1}_y \left(\frac{-V_o}{r}\right) \frac{\tau_2 \cot(\theta)}{2\pi} \Phi^{(h)}\left(\frac{ct}{a\sin(\theta)}\right)$$

$$\vec{E}_{step}{}^{(e)}(r,\theta,t) = \pm \vec{1}_\theta \left(\frac{-V_o}{r}\right) \frac{\tau_2}{2\pi\sin(\theta)} \Phi^{(e)}\left(\frac{ct}{a\sin(\theta)}\right) \qquad (3.D.6)$$

$$\tau_2 = \frac{2}{1+1/\sqrt{\varepsilon_r}} = \tau\sqrt{\varepsilon_r} \equiv \text{dielctric-to-air trans. coeff.}$$

Note that the potential V_o is defined to be the voltage in the dielectric. Because of this, we have included the dielectric-to-air transmission coefficient, τ_2. (Recall that τ is the air-to dielectric transmission coefficient. We have plotted these two step responses for our case of a = 11.3 cm. Time plots are shown in Figure 3.D.4 for a few different values of θ off-boresight in the H- and E-planes. Note that we cannot plot the step response at 0°, because it is a delta function there. Note also that there is little difference between the H-plane and E-plane plots. The only difference is at wider angles, where the difference between $\cot(\theta)$ and $1/\sin(\theta)$ becomes apparent.

To obtain the radiated field, we convolve the above step responses with the derivative of the driving voltage. To drive the antenna, we assume an integrated Gaussian with a peak magnitude of V_o and a risetime of t_d = 50 ps. The time responses are plotted for a few angles away from boresight in the E and H planes, as shown in Figure 3.D.5.

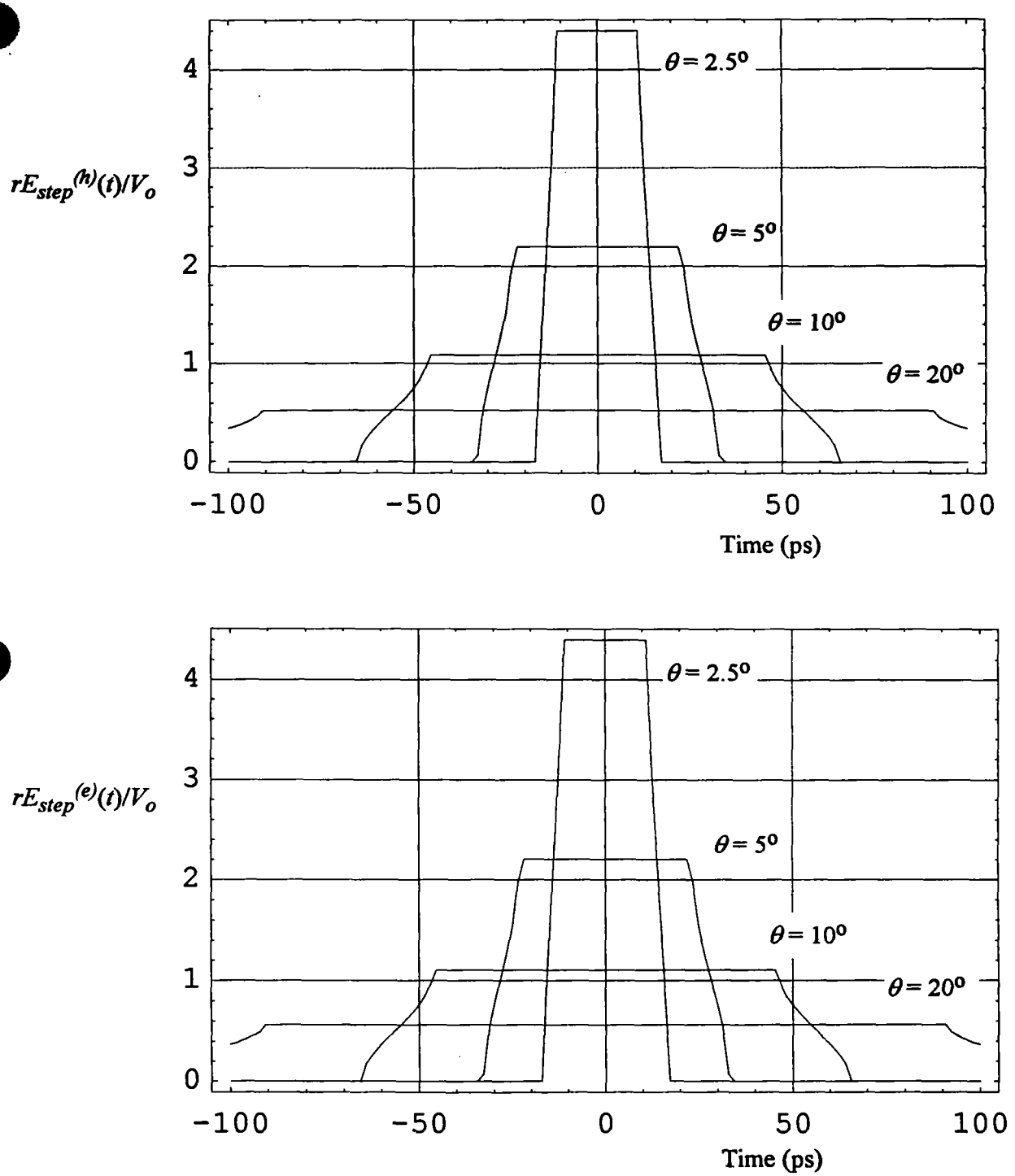

Figure 3.D.4. Step response of the lens IRA in the H-plane (top) and the E-plane (bottom).

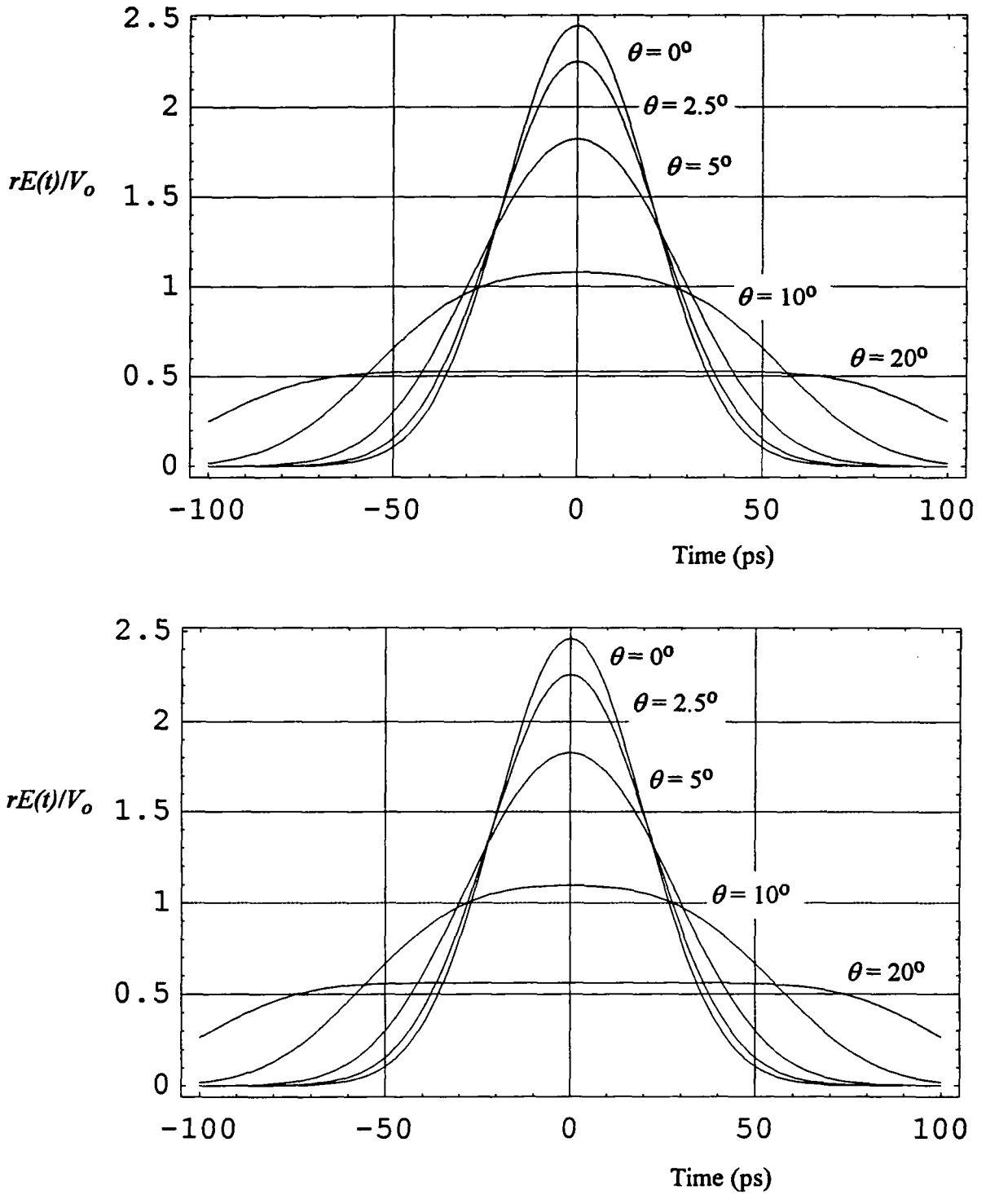

Figure 3.D.5. Fast part of the H-plane (top) and E-plane (bottom) radiated field for the lens IRA.

E. Lens IRA Received Voltage Off-Boresight

We now calculate the received voltage for the lens IRA, just as we did for the reflector IRA in section 2.E. The configuration is once again as shown in Figure 2.E.1. As before, we are interested in this configuration because it will be used to generate antenna patterns.

We need an expression for $h(t)$ both on and off-boresight. To find these, we compare the fast portions of the radiated field, as calculated two different ways. The field radiated on boresight, is just

$$\begin{aligned} E(r,t) &= \frac{1}{2\pi c f_g r} h(t) \circ \frac{dV_{inc}(t)}{dt} \\ h(t) &= h_a \tau \left[\delta_a(t) - \frac{c}{2\ell_1 \sqrt{\varepsilon_r}} \left[u(t) - u(t - 2\ell_1 \sqrt{\varepsilon_r}/c) \right] \right] \\ \tau &= \frac{2}{1+\sqrt{\varepsilon_r}} \equiv \text{air-to-dielectric transmission coefficient} \\ h_a &= 0.85\, a \quad \text{when} \quad f_g \sqrt{\varepsilon_r} = 0.5 \end{aligned} \tag{3.E.1}$$

where ℓ_1 is the length of the horn, r is the distance out to the observer, and h_a is an effective height function that depends upon feed impedance (f_g). Note that $f_g = Z_{feed}/Z_o$ refers to the normalized impedance of the feed *embedded* in the dielectric material. For optimal radiation, $Z_{feed} \times \sqrt{\varepsilon_r} = Z_o/2 = 377/2\ \Omega$. The incident voltage, V_{inc}, is the incident voltage onto the straight section of the TEM feed.

To obtain the off-boresight $h(t)$, we replace the delta function above with a smeared-out version of the delta function. To obtain the smeared-out version, we note that the fast portion of the radiated field on boresight is just

$$E_{step}(r,t) = \frac{V_o}{r} \frac{h_a \tau}{2\pi c f_g} \delta(t) \tag{3.E.2}$$

Furthermore, the off-boresight step responses in the H and E-planes are

$$\begin{aligned} \vec{E}_{step}^{(h)}(r,\theta,t) &= \vec{1}_y \left(\frac{-V_o}{r} \right) \frac{\tau_2 \cot(\theta)}{2\pi} \Phi^{(h)} \left(\frac{ct}{a \sin(\theta)} \right) \\ \vec{E}_{step}^{(e)}(r,\theta,t) &= \pm \vec{1}_\theta \left(\frac{-V_o}{r} \right) \frac{\tau_2}{2\pi \sin(\theta)} \Phi^{(e)} \left(\frac{ct}{a \sin(\theta)} \right) \\ \tau_2 &= \frac{2}{1+1/\sqrt{\varepsilon_r}} = \tau \sqrt{\varepsilon_r} \equiv \text{dielctric-to-air trans. coeff.} \end{aligned} \tag{3.E.3}$$

where the normalized potential functions $\Phi^{(h)}(x)$ and $\Phi^{(e)}(y)$ are defined in the previous section. Comparing the above two expressions, we find they are equivalent on boresight when we replace the delta function in (3.E.1) with a smeared-out delta function defined for both the H- and E-planes. These delta functions, in the E- and H-plane, are just

$$\begin{aligned} \delta^{(h)}(\theta,t) &= \frac{c f_g \sqrt{\varepsilon_r}}{h_a} \cot(\theta)\ \Phi^{(h)}\left(\frac{c t}{a \sin(\theta)}\right) \\ \delta^{(e)}(\theta,t) &= \frac{c f_g \sqrt{\varepsilon_r}}{h_a} \csc(\theta)\ \Phi^{(e)}\left(\frac{c t}{a \sin(\theta)}\right) \end{aligned} \tag{3.E.4}$$

Thus, we find new expressions for the antenna step response, $h(t)$, in the H- and E-planes as

$$\begin{aligned} h^{(h)}(t,\theta) &= h_a\left[\frac{c f_g \sqrt{\varepsilon_r}}{h_a} \cot(\theta)\ \Phi^{(h)}\left(\frac{c t}{a \sin(\theta)}\right) - \frac{\cos(\theta)}{t_{rt}}\left[u(t)-u(t-t_{rt})\right]\right] \\ h^{(e)}(t,\theta) &= h_a\left[\frac{c f_g \sqrt{\varepsilon_r}}{h_a} \csc(\theta)\ \Phi^{(e)}\left(\frac{c t}{a \sin(\theta)}\right) - \frac{\cos(\theta)}{t_{rt}}\left[u(t)-u(t-t_{rt})\right]\right] \\ t_{rt} &= \frac{2\ell_1 \sqrt{\varepsilon_r}}{c} \end{aligned} \tag{3.E.5}$$

These can now be used in the standard expressions for the received voltage. As before, we have,

$$\begin{aligned} V^{(h)}_{rec}(t,\theta) &= \frac{1}{2\pi c f_g r}\, h(t) \circ h^{(h)}(t,\theta) \circ \frac{dV_{inc}(t)}{dt} \\ V^{(e)}_{rec}(t,\theta) &= \frac{1}{2\pi c f_g r}\, h(t) \circ h^{(e)}(t,\theta) \circ \frac{dV_{inc}(t)}{dt} \end{aligned} \tag{3.E.6}$$

These received voltages are calculated for a few angles off-boresight in the H-plane and E-plane, in Figures 3.E.1 and 3.E.2, respectively. Since $\Phi^{(h)}(x)$ and $\Phi^{(e)}(y)$ are the same for our special case of $\alpha = 45^{\circ}$, the two pattern cuts are very similar. The only difference between them is the factor of $\cot(\theta)$ or $\csc(\theta)$ in (3.E.5).

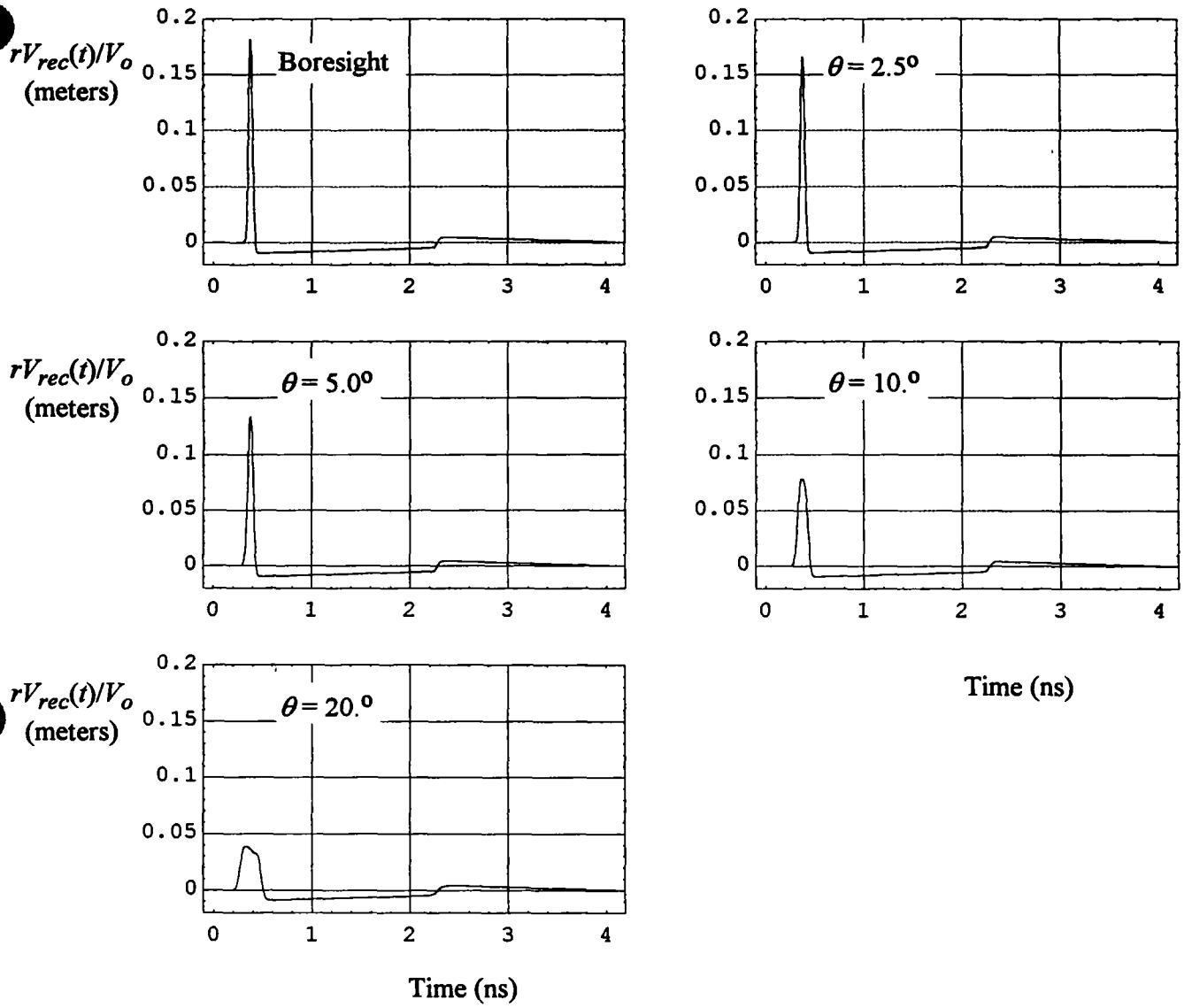

Figure 3.E.1. Received voltage in the H-plane for the lens IRA, with two identical antennas.

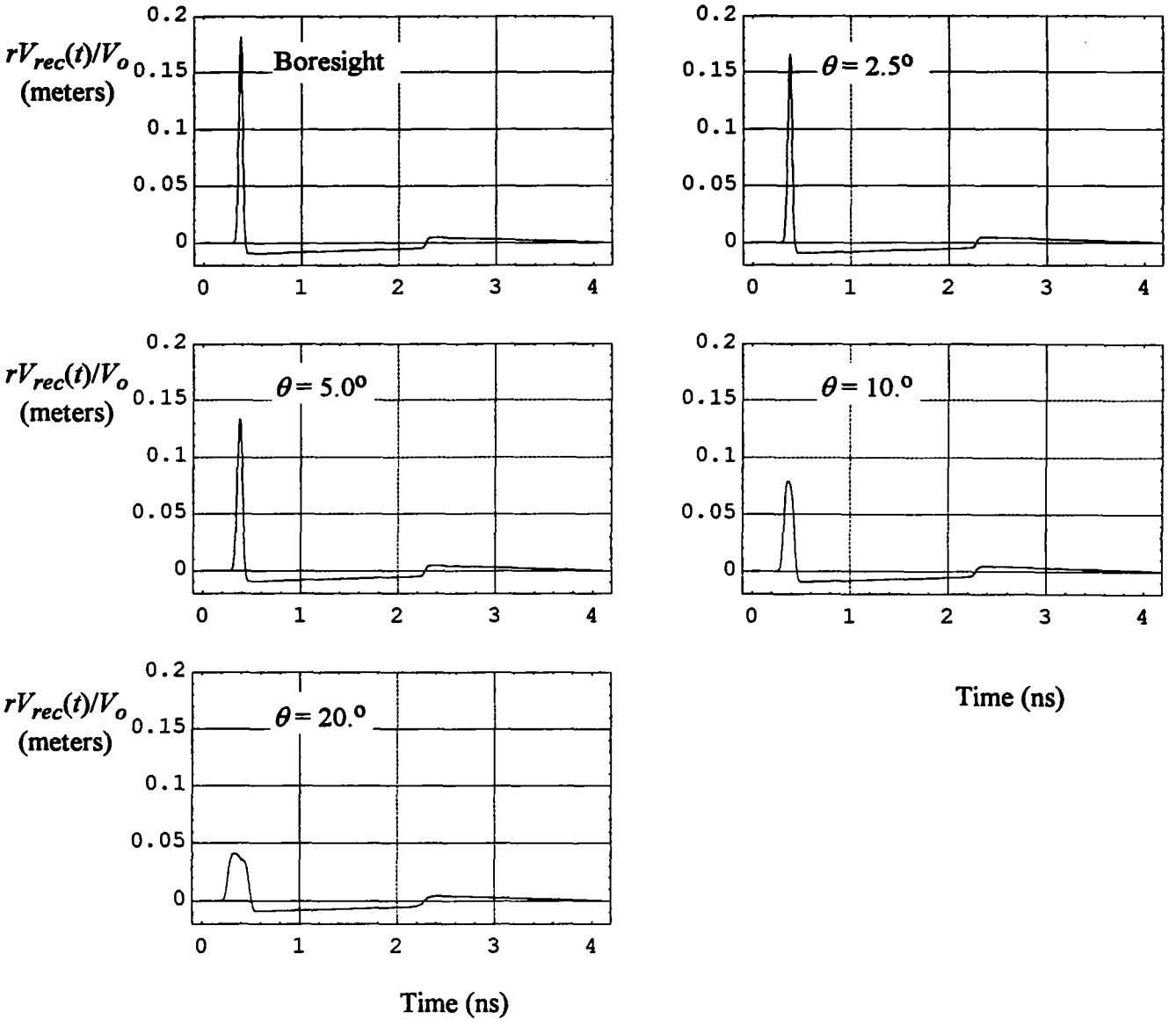

Figure 3.E.2. Received voltage in the E-plane for the lens IRA, with two identical antennas.

IV. Adaptive Noise Filters

In this section we consider improved methods for filtering noise from our data. Our first attempt at solving this problem was to use a modified Butterworth filter, but some small oscillations remained. We consider here additional methods we can try to obtain better results. The problem we wish to solve is actually a very old and well-known problem, and has been considered by many authors. We cannot describe all the methods that are available, but we have selected two that are easy to implement and have led to good results in the past.

The problem can be summarized as follows. One measures an input and output to a linear system as $x(t)$ and $y(t)$, both in the presence of noise. The actual measured waveforms are then

$$\begin{aligned} x_m(t) &= x(t) + n_x(t) \\ y_m(t) &= y(t) + n_y(t) \end{aligned} \tag{4.1}$$

where the subscript m indicates a measured waveform. Let us denote the frequency domain versions of these waveforms with capital letters, e.g., $X_m(\omega)$ and $Y_m(\omega)$. If the noise terms were zero, then one could calculate the impulse response as

$$H(\omega) = \frac{Y_m(\omega)}{X_m(\omega)} = H_m(\omega) \tag{4.2}$$

If there is noise, then one can add a lowpass Butterworth filter, as

$$H(\omega) = \frac{Y_m(\omega)}{X_m(\omega)} G(\omega) \tag{4.3}$$

This is essentially what was done in Phase I. Note the problem, however, that if $X_m(\omega)$ has a null, then we will be dividing by a number close to zero. This will generate a peak in $H(\omega)$ that may not be physical. This peak will show up as a high-frequency oscillation in the time domain. We explore here alternative noise filters that adapt to the actual data to avoid nulls.

The simplest adaptive filter is suggested by Riad [7]. He proposes a filter of the form

$$G(\omega) = \frac{1}{1 + \dfrac{\Phi(\omega)}{|X_m(\omega)|^2}} \tag{4.4}$$

where $\Phi(\omega)$ is a positive function of frequency. For most values of $X_m(\omega)$, $G(\omega)$ is very close to unity. But for values of frequency where $X_m(\omega)$ becomes small, $G(\omega)$ becomes large, thus tending to offset any peaks in the final output $H(\omega)$. The function $\Phi(\omega)$ is most often taken to be

a constant, i.e., $\Phi(\omega) = \lambda$. The value of λ is then optimized for a given set of data. Another form that has been studied is $\Phi(\omega) = \gamma\,\omega^4$, where again γ is a number which must be optimized.

Another adaptive filter is suggested by Nahman[8]. The details of the derivation are somewhat lengthy, so we merely quote the result. The filter one chooses depends on the uncorrected response as

$$G(n,\gamma) = \frac{|X_m(n)|^2}{|X_m(n)|^2 + \gamma|C(n)|^2} \tag{4.5}$$

where we have converted to the discretized form of the transform, with index n. The sequence $c(k)$ is the backward difference operator

$$c(k) = \nabla^2 = \{1,-2,1,0,\ldots,0\} \tag{4.6}$$

which in the frequency domain has a magnitude of

$$|C(n)|^2 = 16\sin^4(\pi n / N), \quad n = 0,\ldots,N-1 \tag{4.7}$$

Once again we see that if $X_m(n)$ is small, then the smoothing filter $C(n)$ becomes important, and $G(n,\gamma)$ becomes large. Note also that there is an error in equation 73 in Reference [8]. It is easily demonstrated by carrying out the math from the step above it, that one gets the result of eqn. (5.5) in this paper.

The approach taken by Nahman is similar to that taken by Riad. To see this, all one has to do is divide eqn. (4.5) by $|X_m(n)|^2$, and one obtains a result in the form of eqn. (4.4).

Finally, we note that there are a variety of least squares-related [9,10] and parametric [11] algorithms. While these may be of interest at a later date, it is likely that the simple algorithms suggested here are sufficient for our requirements.

V. Cable Response

Since cable losses are a significant factor in the design of all our antennas, we consider here a model of pulse propagation along a cable. The simplest model is provided by [12], and it assumes that losses are due primarily to skin effect losses on the center conductor. In this case, the propagation constant along the cable becomes

$$\gamma = \sqrt{\left(K\sqrt{s} + sL\right) sC} \tag{5.1}$$

where L and C are the inductance and capacitance per unit length of the line, and K is the portion of the series impedance due the skin effect. This is found to be

$$K = \frac{1}{2\pi a}\sqrt{\frac{\mu_o}{\sigma}} \tag{5.2}$$

where a is the radius of the center conductor, σ is the conductivity of the wire, and μ_o is the permeability of free space.

After propagating though a cable, it is shown in [12] that the transfer function is just

$$F(s)\ \frac{V_2(s)}{V_1(s)} = e^{-2\sqrt{\beta s}} \tag{5.3}$$

where

$$\beta = \left(\frac{\ell K}{4R_o}\right)^2 \tag{5.4}$$

and R_0 is the characteristic impedance of the line, $R_o = \sqrt{L/C}$. Transforming the above transfer function into the time domain, we find the time domain impulse response of the cable to be

$$f(t) = \frac{1}{\beta\sqrt{\pi}}\left(\frac{\beta}{t}\right)^{3/2} e^{-\beta/t} \tag{5.5}$$

The step response is just the integral of the above impulse response, so we have

$$g(t) = \begin{cases} \operatorname{erfc}\left(\sqrt{\beta/t}\right) & t > 0 \\ 0 & t \le 0 \end{cases} \tag{5.6}$$

where the complementary error function, erfc(t), is defined as

$$\text{erfc}(t) = 1 - \text{erf}(t) = 1 - \frac{2}{\sqrt{\pi}} \int_0^t e^{-x^2} dx \qquad (5.7)$$

We can now plot the impulse response and the step response, $f(t)$ and $g(t)$. We have done so in Figure 5.1.

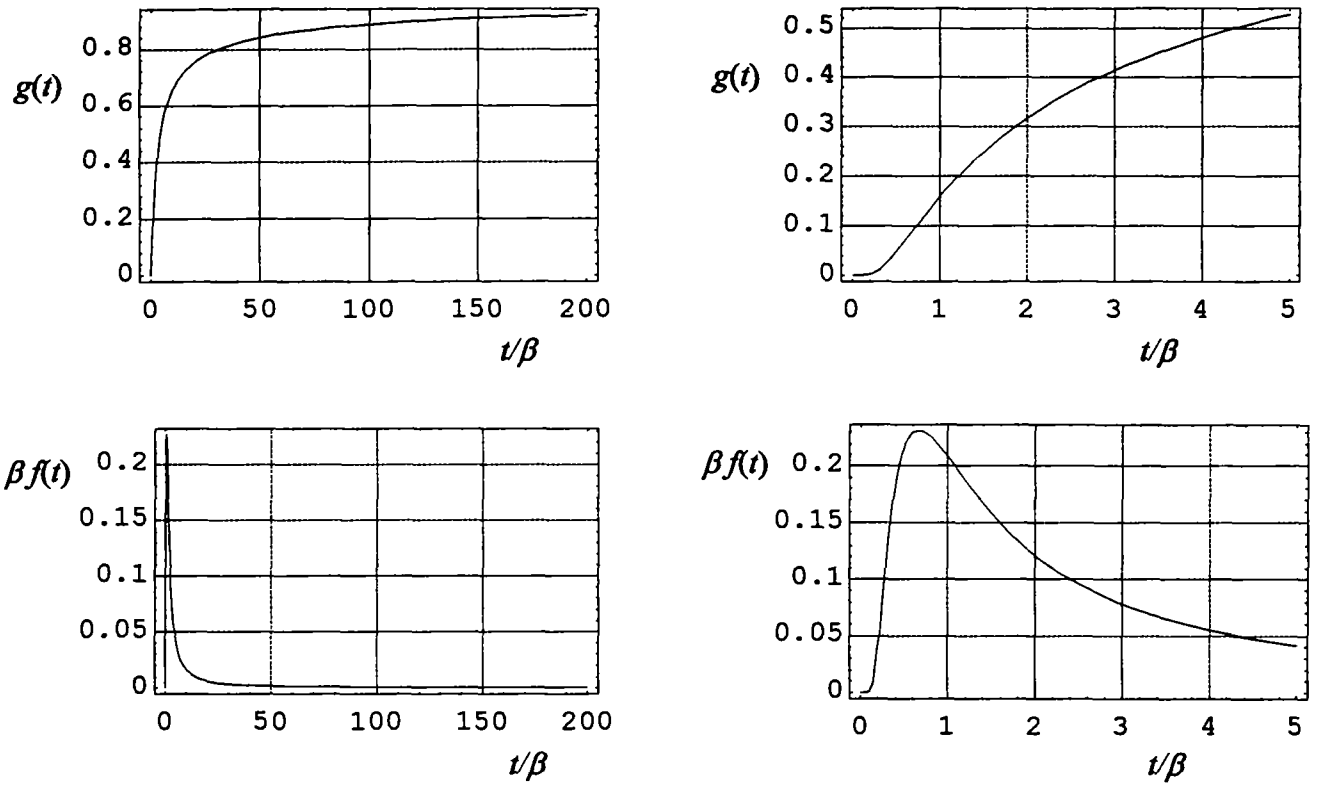

Figure 5.1. Cable propagation step response (top) and impulse response (bottom).

It is interesting to calculate the Full Width Half Max of the impulse response of the cable. By locating numerically the half-voltage points on $f(t)$, we have found the t_{FWHM} to be

$$t_{FWHM} = 1.8 \times \beta \qquad (5.8)$$

If this value is small compared to the risetime of the source, then propagation losses due to this effect can be ignored.

As an example, we consider a 50 Ω cable with silver-coated center conductor ($\sigma = 6.1 \times 10^7$ mho/m), and a center conductor radius of $a = 0.1$ mm. From the above equations, we find $K = 2.3 \times 10^{-4}$ Ω $\text{sec}^{-1/2}$/m. Assuming cable lengths of 1 m and 2 m, we have $\beta = 1.3$ ps and 5.2 ps, respectively. We have convolved the resulting impulse responses with the derivative

of a driving voltage for which t_d = 50 ps (Recall that t_{FWHM} = 0.940 t_d for a Gaussian impulse). The resulting impulse responses are shown in Figure 5.2. After propagating about 2 m, we have lost about half of the peak of *dV/dt*. Since we do not have 2 m of cable in our antennas, the data suggests that other effects are required in order to model the problem completely.

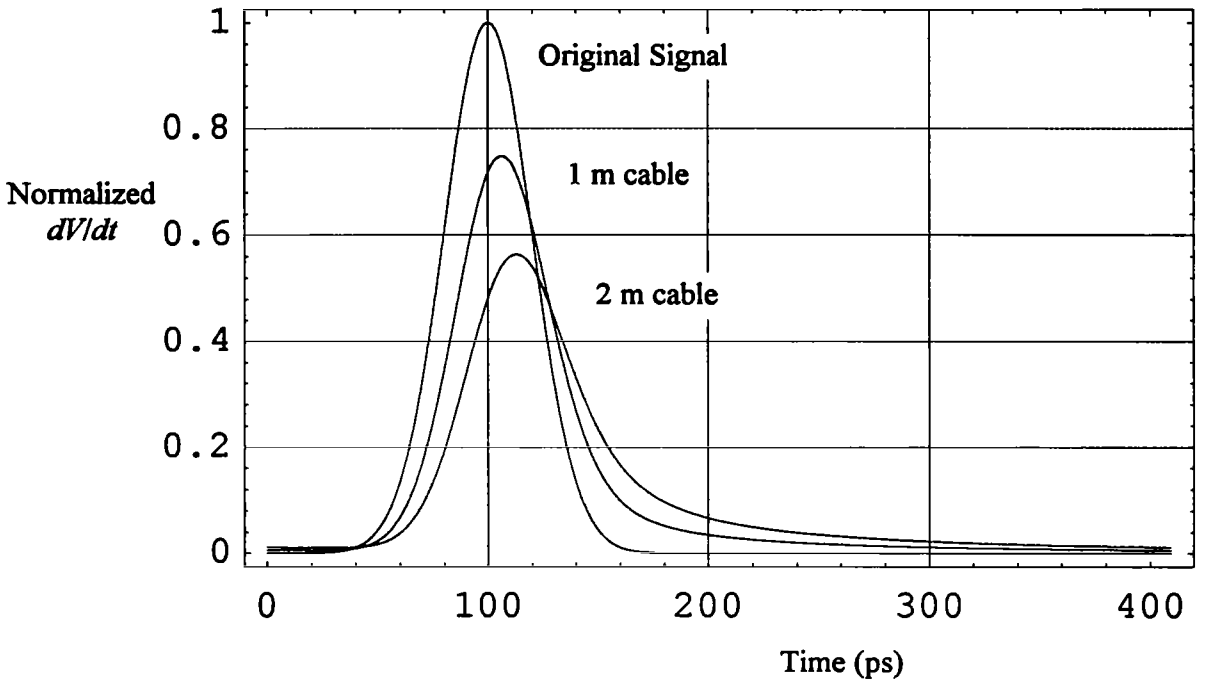

Figure 5.2. The original signal and the signal after propagating through one meter of cable. The peak values are 1., 0.747, and 0.563, and the t_{FWHM} widths are 47.0, 51.8, and 56.3 ps.

VI. Conclusions

We have provided here the design and predictions for a reflector IRA and a dielectric-immersed lens IRA. The dielectric-immersed lens IRA with aspheric lens provides the advantages of reduced Fresnel losses, better match to 50 Ω, and shorter physical length than previous lens IRA designs. New features of the analysis include a calculation of the transient radiated field off-boresight for a 4-wire aperture, and an accurate calculation of the normalized potential for the lens aperture with curved plates. New features of the data analysis include a two-antenna pattern measurement technique in which one antenna is scanned, while the other antenna is held fixed, yielding the angular dependence of the antenna impulse response. Measurements of these antennas will appear in a later note.

Acknowledgments

We wish to thank Dr. Kwang Min of Wright Laboratory / MNMF for funding this work. We also wish to thank Dr. Carl E. Baum, of Phillips Laboratory, for many helpful discussions on this work.

References

1. E. G. Farr and C. E. Baum, Prepulse Associated with the TEM Feed of an Impulse Radiating Antenna, Sensor and Simulation Note 337, March 1992.

2. E. G. Farr and C. A. Frost, Compact Ultra-Short Pulse Fuzing Antenna Design and Measurements, Sensor and Simulation Note 380, June 1995.

3. E. G. Farr and C. E. Baum, The Radiation Pattern of Reflector Impulse Radiating Antennas: Early-Time Response, Sensor and Simulation Note 358, June 1993.

4. C. E. Baum, J. J. Sadler, and A. P. Stone, Uniform Isotropic Dielectric Equal-Time Lenses for Matching Combinations of Plane and Spherical Waves, Sensor and Simulation Note 352, December 1992.

5. G. B. Thomas, *Calculus and Analytic Geometry*, Alternate Edition, Addison-Wesley, 1972, pp. 485-493.

6. E. G. Farr, Off-Boresight Field of a Lens IRA, Sensor and Simulation Note 370, October 1994.

7. S. M. Riad, Instructional Opportunities Offered by the Time-Domain Measurement Technology, Chapter 3 in E. K. Miller (ed.) *Time Domain Measurements in Electromagnetics*, Van Nostrand Reinhold, 1986.

8. N. S. Nahman, Software Correction of Measured Pulse Data, pp. 351-417 in *Fast Electrical and Optical Measurements*, Vol. 1, Martinus Nihjoff Publishers, Dordrecht, The Netherlands, (Distributed by Kluwer Academic Publishers, Boston), 1986.

9. J. Rahman and T. K. Sarkar, "Deconvolution and Total Least Squares in Finding the Impulse Response of an electromagnetic System from Measured Data," *IEEE Trans. Antennas and Propagat.*, Vol. 43, No. 4, April 1995, pp. 416-421.

10. J. V. Candy, G. A, Clark, and D. M, Goodman, Transient Electromagnetic Signal Processing: An Overview of Techniques, Chapter 12 in E. K. Miller (ed.) *Time Domain Measurements in Electromagnetics*, Van Nostrand Reinhold, 1986.

11. D. G. Dudley and D. M, Goodman, Transient Identification and Object Classification, Chapter 13 in E. K. Miller (ed.) *Time Domain Measurements in Electromagnetics*, Van Nostrand Reinhold, 1986.

12. R. L. Wiggington and N. S. Nahman, Transient Analysis of Coaxial Cables Considering Skin Effect, *Proc. of the IRE*, February 1957, pp. 166-174.

13. C. E. Baum, Configurations of TEM Feed for an IRA, Sensor and Simulation Note 327, April 1991.